

The Pléiades Glacier Observatory: high resolution digital elevation models and ortho-imagery to monitor glacier change

Etienne Berthier¹, Jérôme Lebreton¹, Delphine Fontannaz², Steven Hosford², Joaquin M. C. Belart³, Fanny Brun⁴, Liss M. Andreassen⁵, B. Menounos^{6,7}, Charlotte Blondel¹

¹ Université de Toulouse, LEGOS (CNES/CNRS/IRD/UT3), Toulouse, France

² Centre National d'Etudes Spatiales, Toulouse, France

³ National Land Survey of Iceland, Akranes, Iceland

⁴ IGE, Université Grenoble Alpes, CNRS, IRD, Grenoble INP, Grenoble, France

⁵ Section for Glaciers, Ice and Snow, the Norwegian Water Resources and Energy Directorate (NVE), Oslo, Norway

⁶ University of Northern British Columbia, Prince George, BC, Canada

⁷ Hakai Institute, Campbell River, BC, Canada

Correspondence to: Etienne Berthier (etienne.berthier@univ-tlse3.fr)

14

Abstract. Spaceborne digital elevation models (DEMs) of glaciers are essential to describe their health, and their contribution to river runoff and to sea level rise. Publicly available DEMs derived from sub-meter satellite stereo-imagery were, up to now, mainly available in the polar regions and High Mountain Asia. Here, we present the Pléiades Glacier Observatory (PGO), a scientific programme acquiring Pléiades [0.7-m satellite](#) stereo pairs for 140 sites from Earth's glacierized areas. The PGO product consists of [freely-available](#) DEMs at 2 m and 20 m ground sampling distance together with 0.5 m (panchromatic) and 2 m (multispectral) ortho-images. ~~The DEMs are freely available to all registered users whereas ortho-images are available after signing a licence.~~ PGO [stereo acquisitions began](#) ~~commenced~~ in July 2016 in the North Hemisphere and February 2017 in the South Hemisphere. Each site is revisited every five years (cloud permitting), close to the end of the melt season, to measure glacier elevation change with an average uncertainty of 0.49 m (95% confidence level, for a glacierized area of 1 km²), i.e. 0.1 m a⁻¹. PGO samples over 20,000 km² of glacierized terrain which represents about 3% of the Earth's glaciers area. This small sample, however, provides a first order estimate ([within 0.07 m w.e./yr](#)) of the global glacier mass change and its decadal evolution.

1. Introduction

Over the last two decades, the increase in spaceborne satellite imagery archives accelerated our ability to quantify glacier change (Pope et al., 2014; Berthier et al., 2023). Distribution of medium (10-30 m) resolution satellite archives (e.g., from Landsat, [Advanced Spaceborne Thermal Emission and Reflection Radiometer](#) - ASTER) and the open nature of new missions (e.g. the Sentinels from Copernicus), for example, provided imagery to construct improved glacier inventories (Pfeffer et al., 2014; RGI 7.0 Consortium, 2023), spatiotemporal analysis of glacier velocity (Millan et al., 2022) and elevation change (Hugonnet et al., 2021). These global observational products of glacier change are important calibration data to improve projections of future glacier mass change (Rounce et al., 2023).

Glaciology has also benefited from the use of [very-high-resolution \(VHR, i.e., sub-meter\)](#) ~~very high (i.e.-sub-meter)-resolution~~ optical sensors. Contrary to medium-resolution satellite missions, present-day very high resolution satellite missions do not allow a frequent and [continuous](#) global survey of the Earth's glaciers, but these missions are advantageous in a number of ways. The ability to quickly task these satellites provides a means for rapid response following natural disasters (Shugar et al., 2021; Kääb et al., 2021). Their sub-meter resolution translates into superior derived products (e.g. glacier outline, velocity, elevation, snow-line elevation) compared to those obtained from medium resolution imagery. This improved quality is needed to study fine scale processes (Sato et al., 2021; Brun et al., 2016; Loriaux and Ruiz, 2021), monitor small glaciers (Małeckki, 2022), validate similar products derived from coarser images (Andreassen et al., 2022) and also calibrate glaciological mass balance measured in the field (Zemp et al., 2013; Wagnon et al., 2021; Andreassen et al., 2016). With the notable exceptions of the polar regions (Howat et al., 2019; Porter et al., 2018) and High Mountain Asia (Shean et al., 2020), however, access to this very high resolution data has remained limited for the glaciological community.

This article presents the Pléiades Glacier Observatory (PGO), an initiative by the French Space Agency (CNES) and the Laboratoire d'Etudes en Géophysique et Océanographie Spatiales (LEGOS) to facilitate access to very high resolution data (digital elevation models – DEMs – and ortho-imagery) from the Pléiades satellites. We present the coverage achieved since 2016 [for 140 PGO glacierized sites](#) and describe how the freely-available products are derived from raw Pléiades stereo-images. We also assess the quality of the PGO DEMs using [near-contemporaneous](#) accurate [airborne laser scanning lidar](#) data ~~acquired almost simultaneously~~ in Norway and western Canada and evaluate the precision of the elevation change maps that are derived every five years ~~for the 140 PGO glacierized sites~~ [dated sites](#). We conclude by considering how representative the geodetic mass balance derived for these PGO sites is for Earth's glaciers.

62

2. Design of the PGO project

2.1. Pléiades 1A and 1B satellites for glacier monitoring

CNES and Airbus Defense and Space respectively designed and operates the optical satellites Pléiades 1A and 1B (Gleyzes et al., 2012). Pléiades 1A was launched 17 December 2011 and 1B 2 December 2012. The image resolution of the panchromatic and multi-spectral bands are respectively [initially](#) 0.7 m and 2.8 m, [then resampled by the ground segment to 0.5 m and 2 m](#). [Pléiades images have a ~20 km swath, relatively large compared to other VHR satellites \(e.g., 13 km for WorldView-3\)](#). In order to derive DEMs,

70 stereo pairs (respectively ~~or tri-stereo images~~) can be acquired along-track about 40 half a minute
| seconds apart. Compared to earlier stereo sensors (SPOT5-HRS, ALOS-PRISM and TERRA-ASTER Visible
72 and Near-Infrared - VNIR), a clear advantage for snow and ice monitoring is 12-bit encoding of the sensor
| (4096 grey levels) which significantly increases the image contrast ~~over flat and texture-less regions, such~~
74 ~~as snow-covered areas~~ (Berthier et al., 2023).

Early results on several glaciers showed the usefulness of Pléiades data for measuring their topography
76 and its change with time (Berthier et al., 2014; Holzer et al., 2015). The 1-sigma uncertainty of these
Pléiades DEMs is about 1 m over gently sloping areas (Błaszczuk et al., 2019; Berthier et al., 2014). This
78 level of uncertainty is adequate to measure elevation changes, often exceeding reaching several metres,
at seasonal (Belart et al., 2017; Beraud et al., 2023) to inter-annual (Bhattacharya et al., 2021) time
80 scales.

| Airbus operates Pléiades 1A and 1B commercially which does not include building a comprehensive -
82 global archive of images, at least not for glaciers. Furthermore, access to the data is difficult and cost
| prohibitive, especially for users outside of the European Union. These challenges led us to initiate the
84 PGO program in 2016 as a way to monitor a selection of glacier sites around the globe and facilitate
access for the international glaciological community.

86 Despite the 12-bits encoding of the images, we observed saturated pixels for early Pléiades images
| (2011–2015) on well-illuminated slopes (facing toward equator) in the European Alps and Himalaya at the
88 time of image acquisition (10:30 to 11:00h local time). No saturation was observed in the polar regions
due to the lower sun incidence angles. To avoid this saturation in the tropics and mid-latitudes, a request
90 is systematically made to Airbus DS to lower the gain within the 60°N-60°S latitude bands. Technically, it
| consists in requesting to lower the number of time delay and integration (TDI) stages from the default
92 value of 13 to a value of 10. Finally, in an earlier study, we found moderate limited added value of tri-
stereo compared to a standard stereo coverage (Berthier et al., 2014), likely because most of the imaged
94 glaciers are moderately sloped. Tri-stereo coverage being 50% more expensive for the project, PGO
acquisitions are all performed in standard stereo mode.

96 **2.2. Selected glacier targets and acquisitions campaigns**

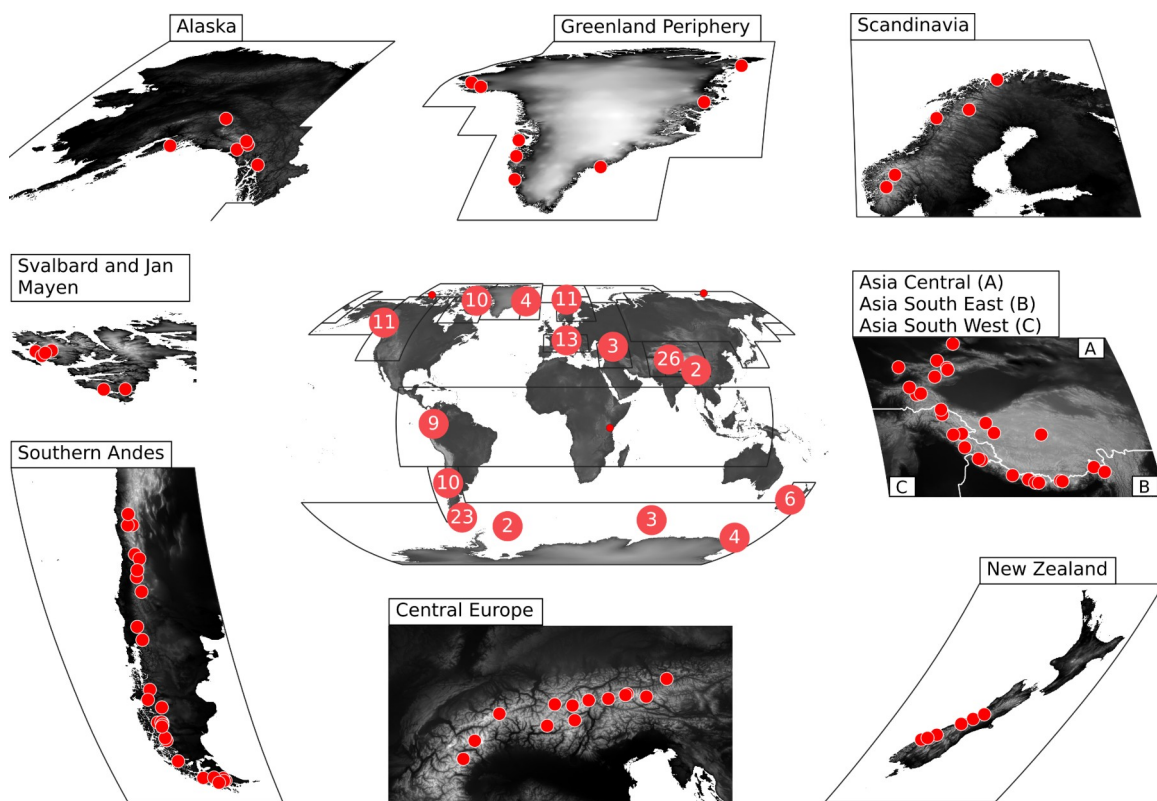
Given the funding available for the PGO, an exhaustive survey of the ~700 000 km² glaciers on Earth is
98 not feasible. Our strategy is, instead, to focus on a discrete number of sites and propose some tailored
acquisitions. In particular, we are careful to task the Pléiades satellites during a time window prescribed
100 by experts in glacier research, in most cases at the end of the summer when the snow cover is the
lowest on and off glaciers. This is important because, when snow is present, the risk of image saturation
102 is higher and, if the snow layer is thick off glacier, the coregistration of the DEMs is more uncertain. Late
summer acquisitions also means that the images and DEMs will often be acquired close in time to the
104 glaciological field measurements or airborne campaigns which facilitates comparisons. Reduced snow
cover also means that most PGO ortho-images should be suitable to update glacier inventories
106 (Andreassen et al., 2022; Paul et al., 2011) and to delineate the snowline, a proxy for the equilibrium line
if observed close to the end of melt season (Pelto, 2010; Rabatel et al., 2013). Images in the PGO
108 database are almost cloud free because any images acquired with more than 10% of clouds are not
| validated and is rejected during the tasking continues. If a cloud free stereo-pair is not obtained during
110 the user-defined time period, the tasking is first extended by a few weeks (if relevant) or/and postponed
to the following year.

112 A PGO site, [based on a user-defined polygon](#), covers typically 100 to 500 km², and generally includes
dozens of glaciers. Site selection was performed following a call to the community through the World
114 Glacier Monitoring Service (WGMS, Zurich), the agency in charge of compiling and disseminating
standardised datasets on glacier fluctuations. The reason to go through the WGMS was that Pléiades
116 repeat DEMs have a high potential to calibrate (field) glaciological mass balance estimates (Zemp et al.,
2013) and also help to assess the regional representativeness of the glaciers monitored in the field. The
118 PGO covers several WGMS benchmark glaciers. We also included iconic glaciers (e.g., Perito Moreno in
Argentina ; Kilimanjaro in Tanzania) and, as much as possible, we attempted to ensure that the PGO
120 samples all main glacierized regions on Earth. The PGO only samples a few sites in the Arctic regions
(including Alaska) because these glaciers are regularly imaged by the ArcticDEM project (Porter et al.,
122 2018). Among the 19 [first order glacier regions defined by the global terrestrial network for glaciers GTN-](#)
[G-first order glacier regions](#) (GTN-G, 2023), only the Russian Arctic is not sampled by the PGO as no
124 request came from the research community for this region. Overall, the PGO acquires imagery over 140
targets (Figure 1, Table 1).

126 For funding reasons, not all [140](#) sites ~~can~~ [could](#) be observed the same year. We thus designed an
acquisition program made of 10 original campaigns, five in each hemisphere. These campaigns occur
128 during the summer and early autumn (i.e. from July to October in the north hemisphere and from
January to May in the south hemisphere). During each of these campaigns, the Pléiades satellites
130 attempted to acquire images over 10 to 30 glacier sites. The first PGO campaign took place in summer
2016 in the northern hemisphere and the last one in summer 2021 in the southern hemisphere.

132 Since July 2021 in the northern hemisphere (and February 2022 in the southern), the PGO has entered
| into “repeat mode”, i.e. stereo coverage is repeated five years after previous acquisitions (cloud
134 permitting). The choice of this 5-yr time lag between acquisitions was driven by (i) the wish to have a
high signal-to-noise ratio on the measurement of the rate of elevation change, and (ii) the consideration
136 that the volume-to-mass conversion factor is not well-constrained for periods shorter than 5-years
(Huss, 2013).

138



140 Figure 1. Map of the distribution of the 140 PGO sites. The central panel shows the number of sites in the main
 142 glacier regions and the peripheral panels highlight the distribution of the sites for a few regions of dense spatial
 144 coverage.

144 Table 1. Summary of the areas and number of glaciers covered during the first 10 PGO original campaigns. NH
 146 stands for Northern Hemisphere, SH for Southern Hemisphere. See also Table 3 for the distribution of sites
 among the 19 GTN-G first order glacier regions. **The columns "total and glacier areas" correspond to the full
 coverage. The real area coverage by PGO is in fact slightly lower due to data gaps in the DEMs.**

Campaign	Number of sites	<u>Number of stereo pairs</u>	Total area km ²	Glacier area km ²	Number of glaciers*	<u>Number of stereo pairs</u>
2016 NH	18	<u>30</u>	7163	2514	771	<u>30</u>
2017 SH	14	<u>28</u>	4970	1819	813	<u>28</u>
2017 NH	29	<u>52</u>	11,262	4434	1469	<u>52</u>
2018 SH	9	<u>22</u>	3671	1535	365	<u>22</u>
2018 NH	13	<u>26</u>	4719	1826	573	<u>26</u>
2019 SH	5	<u>23</u>	3352	1911	221	<u>23</u>
2019 NH	14	<u>34</u>	6229	1909	1019	<u>34</u>
2020 SH	12	<u>21</u>	4338	1491	670	<u>21</u>
2020 NH	14	<u>27</u>	5276	2065	784	<u>27</u>
2021 SH	12	<u>19</u>	3509	1870	125	<u>19</u>
Total	140	<u>282</u>	54,489	21,374	6810	<u>282</u>

* Counting only glaciers for which at least 50% of the area is covered.

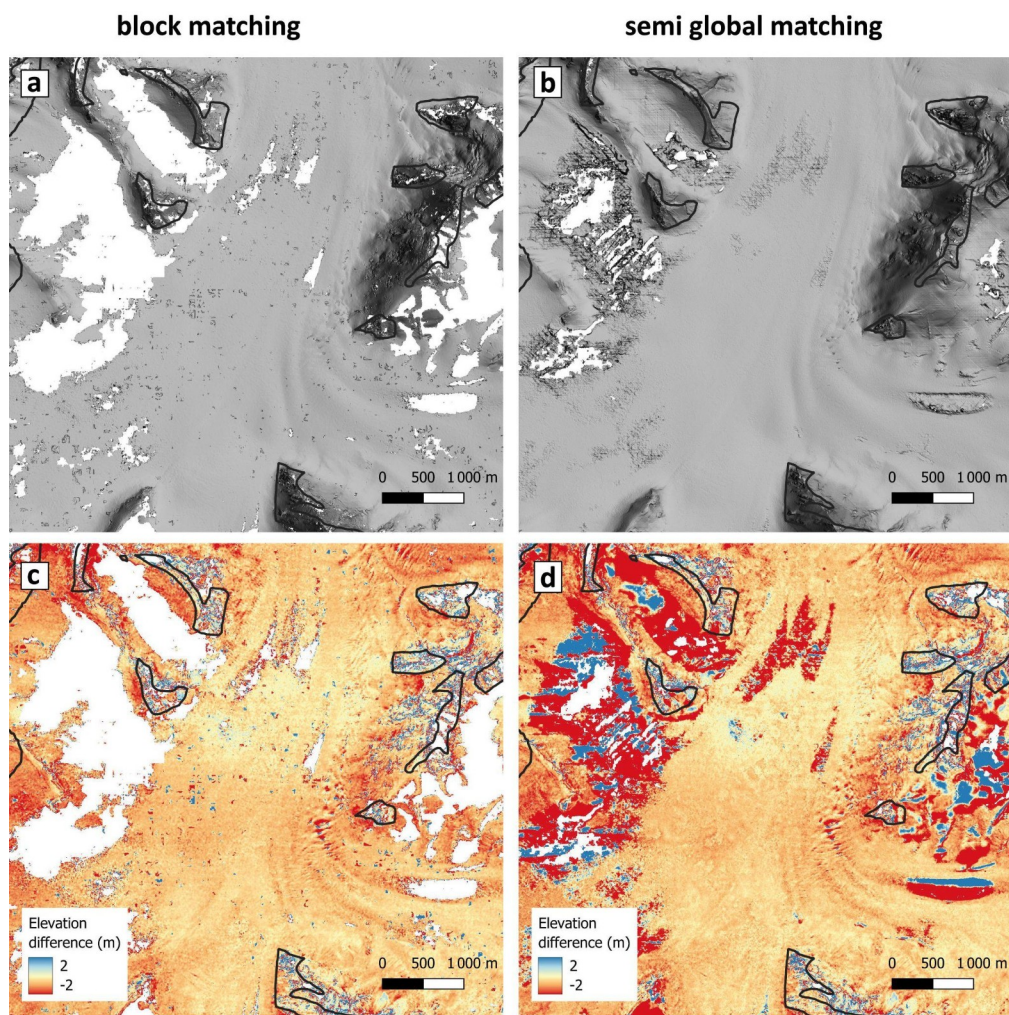
2.3. The PGO products

150 The PGO products consist of the DEMs and related ortho-images derived automatically from the [stereo](#)
151 [image pairstereo-pair](#), and the 5-year maps of elevation difference calculated once a PGO site has been
152 observed again by the Pléiades satellites.

2.3.1. DEMs and ortho-images

154 Airbus Defense and Space provides Pléiades ~~stereo~~ [stereo](#)-pairs at the “primary” processing level. We then
155 generate DEMs and ortho-images using the Ames Stereo Pipeline (ASP) (Beyer et al., 2018 ; [Shean et al.,](#)
156 [2016](#)), version 3.0.0, release 2021-10-05 (<https://github.com/NeoGeographyToolkit/StereoPipeline>). ASP
157 is a suite of free and open source tools designed for processing stereo images captured from satellites
158 and other platforms. It is extensively used in glaciology to generate DEMs from [Maxar](#)
159 [WorldView/GeoEye Worldview](#) (Shean et al., 2016; Willis et al., 2015), ASTER [VNIR \(Advanced-](#)
160 [Spaceborne Thermal Emission and Reflection Radiometer\)](#) on board TERRA (Brun et al., 2017; Shean et
161 al., 2020), ~~and~~ Pléiades (Marti et al., 2016; Deschamps-Berger et al., 2020) [and Planet SkySat-C \(Bhushan](#)
162 [et al., 2021\) imagesatellites](#).

A key step for the generation of a DEM is the correlation between the two images of the stereo-pair.
164 Several algorithms are available in ASP that can lead to different results. Deschamps-Berger et al. (2020)
165 showed that the choice of the photogrammetric options, and in particular the correlator, has an impact
166 on the precision and completeness of the elevation difference over stable terrain and snow-covered
167 areas. We used their preferred set of photogrammetric options, based on the Semi-Global Matching
168 (SGM) correlator (Hirschmuller, 2008). SGM has the advantage of providing [enhanced DEM detail/quality](#)
169 [and fewer data gapsa highly resolved topography and a limited amount of data gaps](#). However, we
170 observed that in some cases (Figure 2), SGM tended to fill the DEM with noisy data in textureless areas
171 of the images (cast shadows, areas covered with fresh snow, [and in the case of Fedchenko in Figure 2](#)
172 [saturated image saturations](#)). For this reason, we also processed the stereo-pairs using the block-
173 matching (BM) correlator with a set of processing parameters taken from (Willis et al., 2015; Marti et al.,
174 2016). We provide both versions (SGM and BM) and leave it to the user with their local knowledge of the
175 study area to decide which version of the DEM (or a combination of both) is the most appropriate for a
176 given study. We produced 2 and 20 m DEMs from the native point clouds generated by ASP. The 20-m
177 DEM is a smoother version that can be useful for testing some methodologies on smaller files and for
178 generating more complete ortho-images as it contains less data gaps.



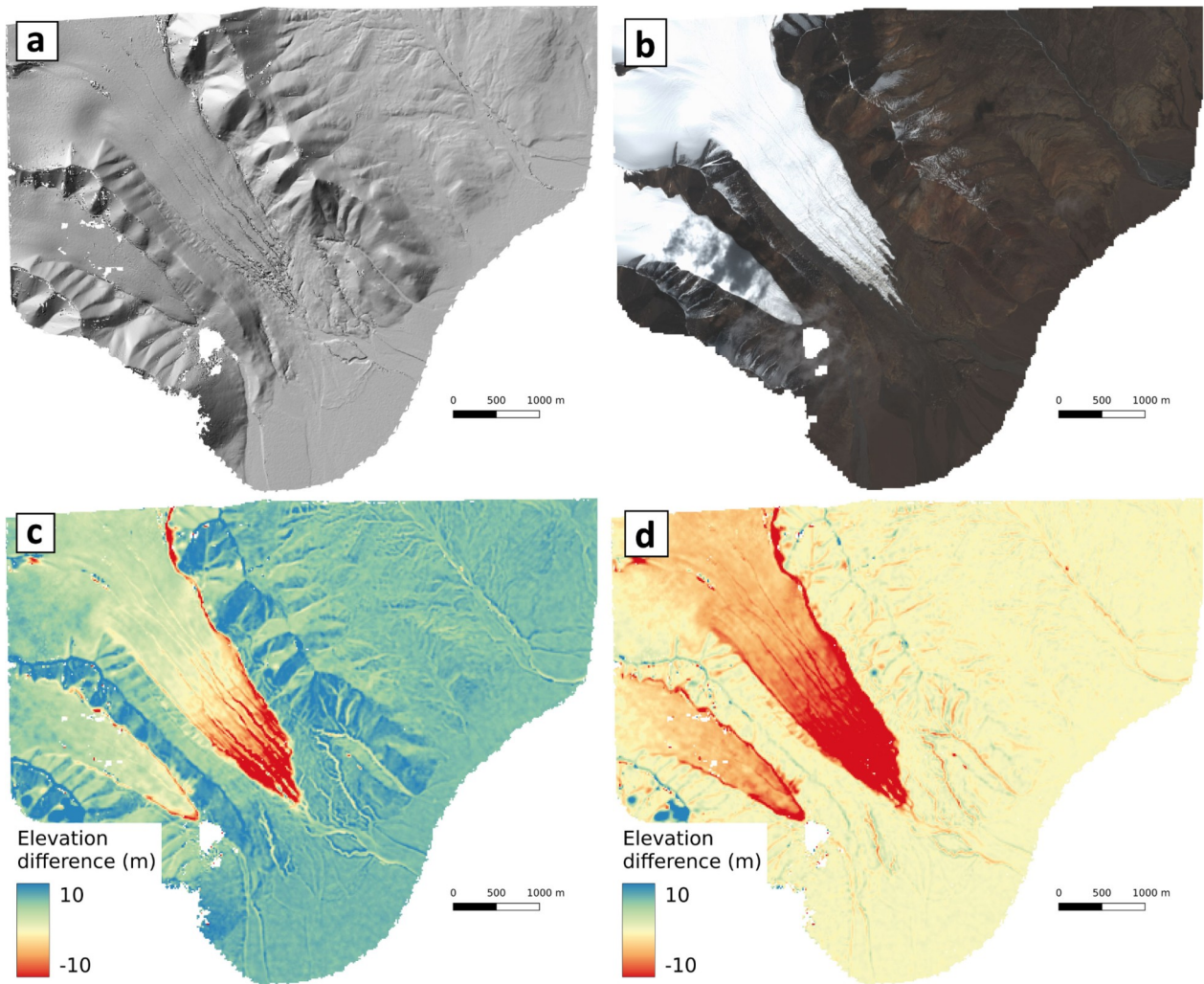
180 **Figure 2. Comparison of the Pléiades 2-m DEMs derived using the block-matching BM (left) and semi-global**
 182 **matching SGM (right) algorithms of the Ames Stereo Pipeline (ASP) for the upper accumulation area of**
 184 **Pléiades DEMs. Note that the locations where data gaps are present in the block-matching BM DEMs (white**
 186 **areas in panels a and c) correspond to unrealistically high/low values in the semi-global matching SGM elevation**
difference map (panel d). These gaps result mostly from saturation in the images.

In our workflow, 0.5 m panchromatic and 2 m multispectral ortho-images are generated using the 20-m
 188 DEM. Pansharpended images (i.e. multispectral images at 0.5 m resolution) are not calculated and
 archived due to file storage limitations. These pansharpended images, however, could easily be generated
 190 by the user using freely available tools such as *pansharp* in ASP or *otbcli_Pansharpening* in the Orfeo
 ToolBox (<https://www.orfeo-toolbox.org/>).

192 The official absolute geolocation accuracyNative-geolocation-performance is 8.5 m (CE90, Circular Error
 at a confidence level of 90 %) for Pléiades-1A and 4.5 m for Pléiades-1B (Lebègue et al., 2015) without
 194 ground control points (GCPs). Further, Pléiades DEMs derived without GCPs can be biased in height by as
 much as 10 to 20 m. To avoid such large horizontal and vertical shifts and to ensure an improved
 196 consistency of the PGO database, all DEMs were are coregistered to the Copernicus GLO-30 DEM (GLO-
 30) using a publicly available implementation by Shean et al. (2016)
 198 (<https://github.com/dshean/demcoreg>) of the Nuth and Kääb (2011)'s algorithm (Shean et al., 2023) .
 GLO-30, an edited version of the TanDEM-X DEM, has a 30-m ground sampling distance and was chosen

200 as a reference DEM because it is currently the best global void free DEM publicly available (Franks and
| Rengarajan, 2023). [According to ESA and AIRBUS \(2022\), Its absolute vertical accuracy is better than 4m](#)
202 [\(90% linear error\) and its absolute horizontal accuracy is better than 6m \(90% circular error\)](#). Given the
time lag between the radar images used to produce the TanDEM-X DEM (2011 to 2015, (Rizzoli et al.,
204 2017)) and the PGO acquisitions, coregistration was performed on stable terrain, masking out glaciers as
| inventoried in the RGI v6.0 (RGI Consortium, 2017). For a few test sites, we found that the [3D translation](#)
206 [vectors](#)~~coregistration vectors~~ were almost unchanged when using the 20 m instead of the 2 m DEM.
| Hence, the [3D translation shift](#) vectors were computed using the 20 m DEMs [only](#) (a ground sampling
208 distance closer to the one of GLO-30) and the shifts were applied to all PGO products (2-m and 20-m
| DEMs and all ortho-images). [Coregistration to GLO-30 is performed separately for BM and SGM DEMs.](#)

210 Figure 3 shows one of the PGO products (DEM and ortho-images) and the elevation difference to GLO-30
before and after coregistration for a portion of the Purogangri ice cap over the Tibetan Plateau. An
212 example of the [product metadata report](#)~~fact sheet~~ that accompanies each PGO product is available in
[Appendix A1](#).



214

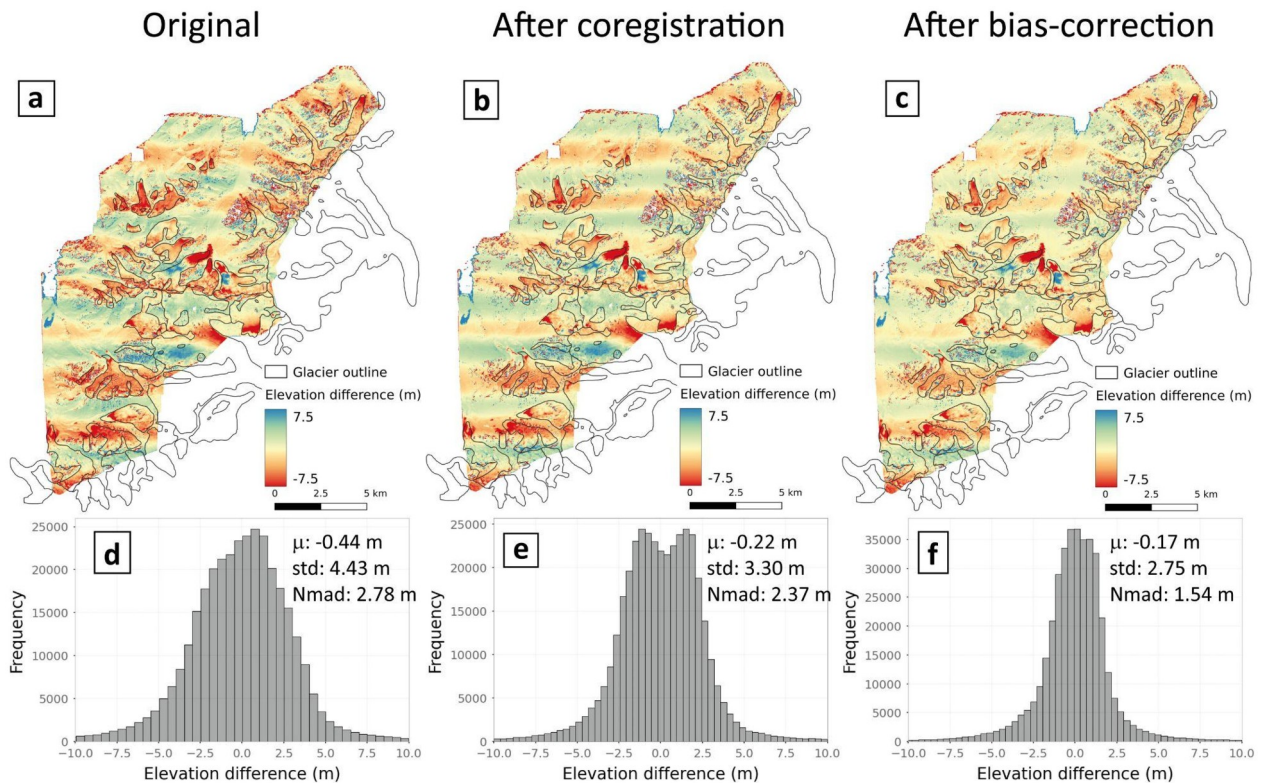
Figure 3. A sample PGO product for the Purogangri ice cap over the Tibetan Plateau (PGO ID: 2018-10-03_0458515_Purogangri_ASC). (a) Shaded relief image of the block-matching BM-DEM; (b) multi-spectral 2-m ortho-image © CNES 2018, Distribution Airbus DS ; (c) Elevation difference of the Pléiades DEMs with the Copernicus 30 DEM prior (c) and after (d) coregistration. For this specific case, the shift vector of the PGO DEMs to GLO-30 were: $d_{East} = -1.8$ m ; $d_{North} = 4.8$ m ; $dZ = -6.6$ m. Coregistration reduced the normalized median absolute deviation (NMAD) off glacier from 0.81 m to 0.48 m.

222 2.3.2. Maps of elevation changes

Once Pléiades acquisitions are repeated over a PGO-site is observed again, we generate DEMs from the most recent Pléiades imagery and compare these to the older DEMs to map five (sometimes six or more) years of glacier elevation change (Figure 4). This is achieved in two steps: first the most recent Pléiades DEM is coregistered to the older one (derived at the same ground sampling distance and using the same correlator) on the stable terrain, using the demcoreg package, as described above, the implementation by D. Shean of the Nuth and Kääb (2011)'s algorithm. Next, remaining spatially-coherent elevation biases are corrected by fitting a fifth order polynomial in the across-track direction (Gardelle et al., 2013) and a spline fit along-track (Falaschi et al., 2023). The latter is needed to correct low-frequency undulating biases due to the unmodeled attitude error ("jitter") jitter of the Pléiades satellite platform at a frequency of about 1 Hz (Deschamps-Berger et al., 2020). These along-track biases are not systematic and have a typical amplitude of 1–2 m and a wavelength of about 4 km.

234 The jitter is especially strong for Pléiades 1B since the year 2021 due to an issue with the satellite
 236 platform. These across-track and along-track corrections are only efficient if there is a sufficient amount
 of well-distributed stable terrain around the glaciers. In the case of the Tuyuksu site (Figure 4),
 successive corrections allow reducing the dispersion of the residuals by almost a factor of two, e.g. the
 238 normalized median absolute deviation (NMAD) is lowered from 2.8 to 1.5 m. The along-track undulations
 are not entirely removed (Figure 4c), however. Thus, we invite the users to check statistics and carefully
 240 check the -do visual inspection of the difference maps on stable terrain to assess as an indicator of the
 quality of the corrections (see also Figure A3 in Berthier et al., in press).

242



244 **Figure 4. PGO elevation difference map before and after two corrections** Processing steps to generate the PGO-
 elevation change maps on the Tuyuksu (Central Asia) site in Kazakhstan. The upper panels (a, b, c) show the
 246 elevation differences maps from August 2016 to August 2021 and the lower panels (d, e, f) the distribution of the
 elevation differences off glaciers. Maps and histograms are shown before coregistration (a, d), after
 248 coregistration (b, e) and after bias corrections (c, f). (PGO ID: 2016-08-27_0545099_Tuyuksu_ASC ; 2021-08-
 21_0546043_Tuyuksu_ASC, both derived from Pléiades 1B images).

250 Two, three (and sometimes more) stereo pairs are often needed to cover entirely a single PGO site in a
campaign year. After five years, we thus generate the elevation change maps for all possible pairs of
 252 overlapping DEMs, at 2 and 20 m ground sampling distance and for the two algorithms (SGM and BM,
 Fig. 2). Hence, numerous elevation change maps are computed and we leave it to the users to decide
 254 which combination works best for their needs. Basic statistics are provided for each elevation change
 map (e.g., standard deviation and NMAD off glacier, as in Figure 4) to guide the users in their choice.

256

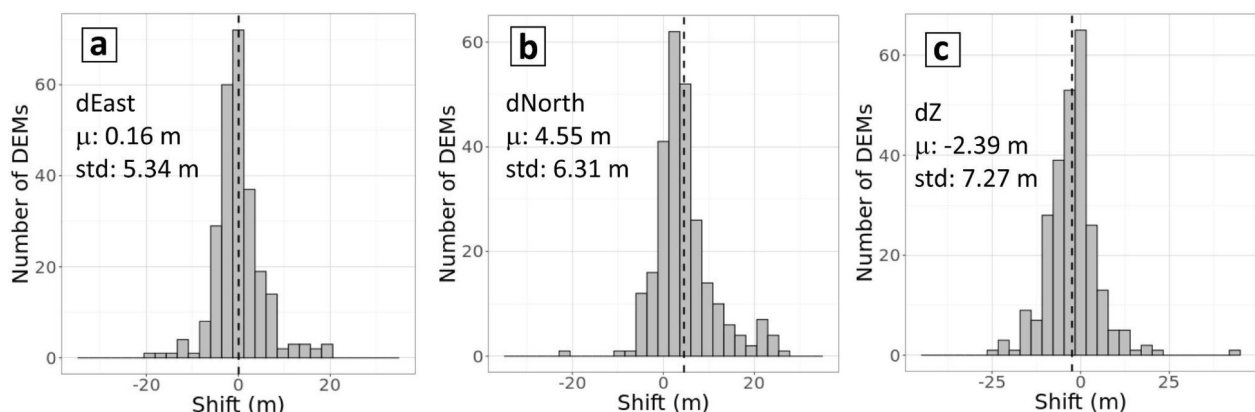
3. Evaluation of the PGO datasets

258 3.1. Evaluation of the DEMs

3.1.1 Quality of the coregistration to GLO-30

260 We assess the quality of the coregistration of 259 PGO DEMs to GLO-30 (Figure 5) off-glacier. The spread
of the residuals are similar in both easting and northing directions with standard deviations of 5 to 6 m,
262 and the standard deviation is slightly larger than 7 m in the vertical direction. The median shift is almost
0 m in easting direction, whereas the PGO DEMs are slightly shifted (4.5 m) toward the North compared
264 to GLO-30. This northward shift is larger for DEMs derived from Pléiades 1A images (5.8 m) than from
Pléiades 1B (3.2 m) and is especially strong at high (north and south) latitudes, reaching up to 20 m at
266 80° North in Svalbard. We have no explanation for this small systematic northward shift which is under
investigation at the French Space Agency (CNES). PGO DEMs are, on average, 2.4 m lower than GLO-30.
268 This vertical shift could be due to winter snow affecting the GLO-30 (derived from individual Tandem-X
DEMs acquired year round) but not affecting the PGO DEMs, acquired only in summer. This vertical
270 offset is larger for DEMs derived from Pléiades 1B images (3.9 m) than from Pléiades 1A (1.1 m) We note
that these horizontal and vertical shift values (mean/standard deviation) do not represent the absolute
272 geolocation performance of the Pléiades DEMs as they are also influenced by any mis-registration of
GLO-30 itself.

274

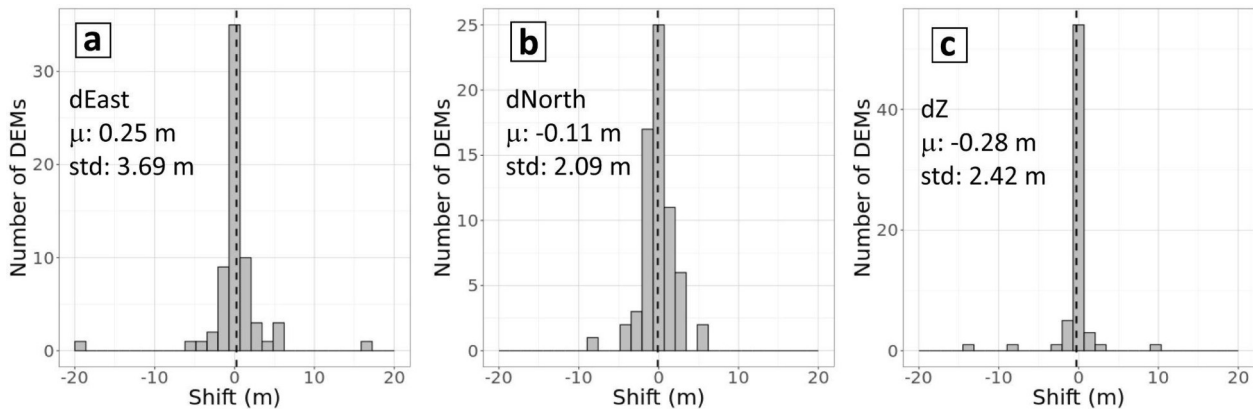


276 **Figure 5. Distributions of the shifts in the easting (a), northing (b) and vertical (c) directions between 259 PGO
DEMs acquired between 2016 and 2021¹² (10 first campaigns) and GLO-30 off-glacier. “ μ ” stands for the mean,
278 “std” for the standard deviation. The figure only shows the histograms for the block-matching 20 m BM-DEMs.
The figure shows translation components for the block-matching DEMs, as the mean and standard deviation for
280 the semi-global matching DEMs were nearly identical. For the semi-global matching DEMs (not shown), the mean
and standard deviation of the shifts are almost unchanged, within a few tenth of centimetres.**

282 Coregistration to GLO-30 failed or led to unreliable horizontal shifts (> 30 m) for about 10% of the sites.
Examples of problematic sites include Livingstone Island (Subantarctic and Antarctic Islands) where GLO-
284 30 displays large artefacts, possibly due to errors during the unwrapping of the TanDEM-X
interferograms. Hence for seven DEMs out of nine on this Island, we applied no coregistration.
286 Coregistration also failed in a few cases where very limited stable terrain was available (e.g., on Balleny
Islands around Antarctica). When coregistration failed or was judged unreliable, the Pléiades DEM were
288 left unchanged (i.e. not shifted) and the unsuccessful coregistration was identified on the metadata
sheet accompanying each PGO product.

290 3.1.2 Comparison of close-in-time PGO DEMs in their overlapping areas

As several Pléiades DEMs are sometimes needed to cover a PGO site, they include overlapping areas
292 where the DEMs acquired a few days/weeks apart can be compared. These overlapping areas provide an
opportunity to assess the performance of the coregistration, the so-called “triangulation” in Nuth and
294 Kääb (2011). Indeed, after coregistration to GLO-30, we expect two overlapping Pléiades DEMs to be
well-coregistered, and residual shifts between the DEMs can be interpreted as residual coregistration
296 errors (Figure 6).



298 **Figure 6. Distributions of the shifts in the easting (a), northing (b) and vertical (c) directions between**
figure 5 but for the the PGO DEMs over their overlapping portions (n=64). We only show the results for the 2 m
300 **block-matching BM-DEM. Results are very similar for the semi-global matching DEMs and at both resolutions (2**
m and 20 m).

302 The mean residuals are very close to 0 m in all directions and the standard deviations range from 2 to 4
m. This reflects the quality of the PGO DEM coregistration with the reference GLO-30 product to GLO-30.
304 We note that a few PGO DEMs show relative co-registration errors/residual shifts of over 10 m. They
correspond to sites in areas of high relief (e.g., glacier Fedchenko in Tadjikistan or Makalu in Nepal)
306 where GLO-30 is subjected to large errors.

3.1.3 Evaluation of the PGO DEMs using near-contemporaneous simultaneous lidar data

308 In Norway and western Canada, three independent airborne lidar campaigns acquired data within less
than 1 day of a Pléiades stereo acquisition (Table 2) ~~airborne lidar campaigns fortuitously acquired data~~
310 ~~with a separation time of one day or less of Pléiades stereo collection (Table 2).~~ This ideal situation
allows us to evaluate the performance of the PGO DEMs because of negligible glacier elevation change
312 on all surfaces (glacier, snow, permafrost). The simultaneity of the surveys allows comparison of the
uncertainties of the PGO DEMs on and off glacier, an important aspect as, in general, one has to assume
314 that the off glacier terrain is representative of the glacier terrain (Hugonnet et al., 2022). Hence, the
elevation difference directly reflects the uncertainties of the PGO DEMs. Uncertainties based on
316 repeated lidar acquisitions over stable terrain typically yield errors (~0.1 m) that are almost one order of
magnitude smaller than those of the PGO DEMs, ~~hence they are neglected here~~ Hence the elevation
318 difference mainly reflects the uncertainties of the PGO DEMs, although ALS errors can be higher than 0.1
m in steep terrain. Details about the western Canada lidar surveys can be found in Pelto et al. (2019).
320 ~~The simultaneity of the surveys allows comparison of the uncertainties of the PGO DEMs on and off~~
glacier, an important aspect as, in general, one has to assume that the off glacier terrain is
322 representative of the glacier terrain (Hugonnet et al., 2022). For this comparison, we use the final PGO
DEM, coregistered to GLO-30.

324 The lidar pointclouds were ~~triangulated and linearly~~ interpolated into 1 m gridded DEMs using ASP's
 routine *point2dem*. For the comparison, we coregistered each PGO DEM (i.e., BM and SGM) with each
 326 synchronous lidar (~~Shean et al., 2016; Nuth and Kääb, 2011~~). The DEM coregistration was done using the
 RGI v6.0 (RGI Consortium, 2017) glacier inventory as a mask to define the stable terrain because this is
 328 the only inventory available for coregistration on all PGO sites, and in this process the lidar DEMs were
~~bilinearly re-sampled to 2x2 m in order to match the resolution of the Pléiades DEMs.~~ Observed
 330 elevation differences (Figure 7) are in general near 0, but there are also some artefacts and differences
between BM vs SGM products.

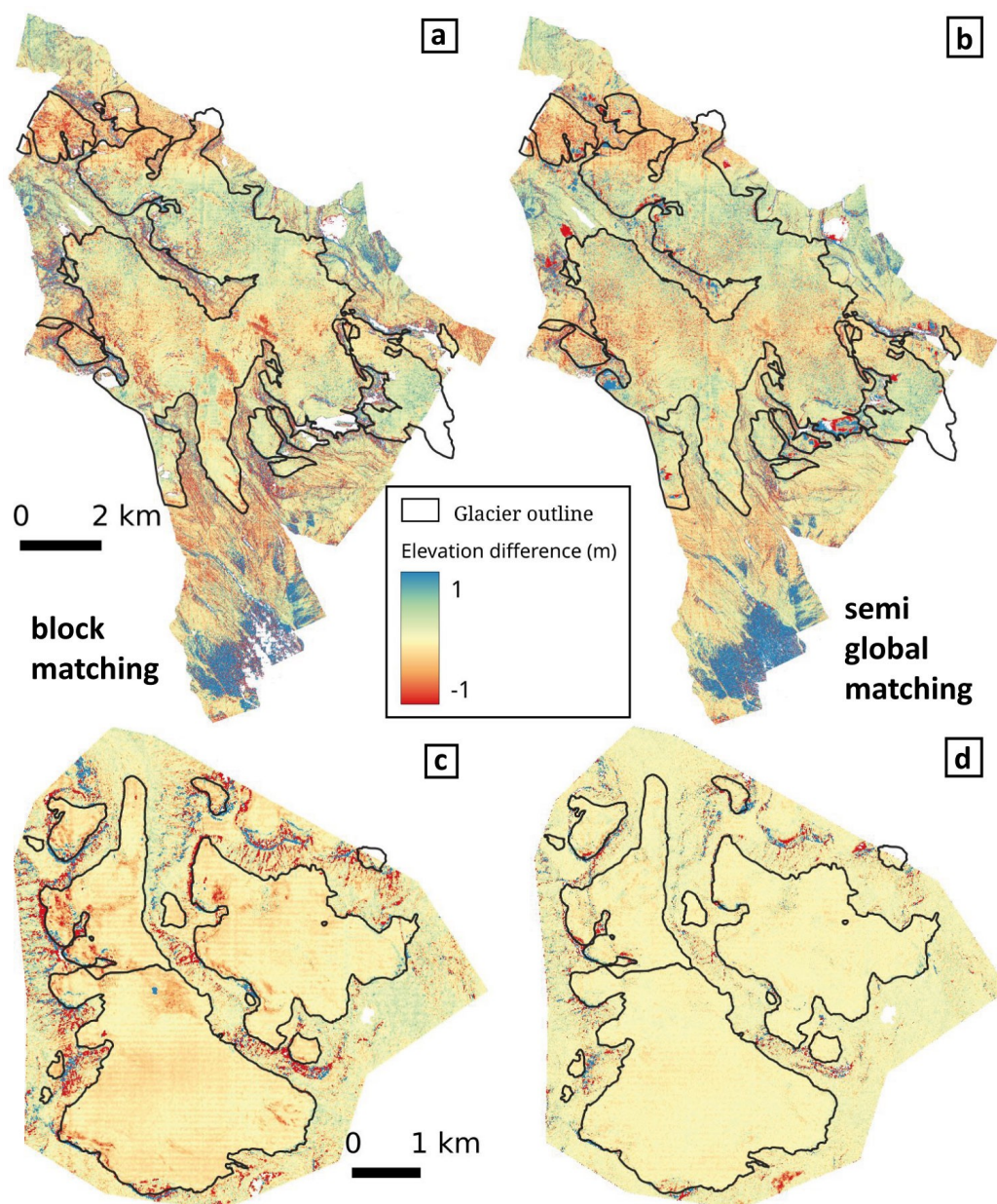
332 ~~Further~~To evaluate the quality of the PGO DEMs, we calculated different statistics to characterise DEM
 uncertainties, based on the maps of elevation difference between Pléiades and lidar (Fig. 7): NMAD off-
 334 glacier and on-glacier, median off-glacier and on-glacier (Table 3). For these statistics, on- and off- glacier
 terrain was classified using high resolution glacier outlines manually digitized on the Pléiades
 336 orthoimages and a hillshade representation of the lidar DEMs. This improved glacier inventory was
needed as RGI outlines were outdated and we wanted to have the best possible separation between
 338 glacier and stable terrain.

Table 2. Characteristics of the lidar surveys used to evaluate the PGO DEMs.

Region	Surveyed glaciers	Glacier area (km ²) <u>∟</u> <u>evaluation</u> <u>area</u> <u>(km2)</u>	Date PGO/lidar YYYY-MM-DD	PGO /Geostore ID	Lidar <u>density</u> p/m ²	Avg Slope on/off glacier
Western Canada	Peyto	47.0 / <u>94.6</u>	2016-09-13 / 2016-09-13	2016-09-13_1912075_Wapta_WNA / DS_PHR1B_201609131912075_FR1_PX_W117N51_0616_02636	1	13°/28°
North Norway	Langfjordjøkelen	6.4 / <u>17.1</u>	2018-09-01 / 2018-09-01	NaN / DS_PHR1B_201809011030275_FR1_PX_E021N70_0604_01124*	2	12°/31°
South Norway	Hellstugubreen, Gråsubreen, Vestre Memurubreen, Austre Memurubreen	19.7 / <u>42.7</u>	2019-08-27 / 2019-08-26	2019-08-27_1102544_Jotunheimen_SCA / DS_PHR1B_201908271102544_FR1_PX_E008N61_0615_01712	2	11°/26°

340 *Langfjordjøkelen was surveyed by the PGO one year earlier, 8 September 2017. This 2018 Pléiades
 stereo pair was not acquired as part of the PGO, this is why we only provide the ID of the Pléiades stereo
 342 pair in the Geostore Airbus D&S catalogue. The processing used for this non-PGO DEM was identical to
PGO DEMs.

344



346

Figure 7. Map of elevation differences between PGO and Lidar DEMs acquired the same day over Peyto Glacier
 348 (13 September 2016, Canada, panels a and b) and one day apart over Hellstugubreen (26 and 27 August 2019,
 Norway, panels c and d). The left column shows the two block-matching DEMs, the right column the semi-global
 350 matching DEMs. We do not show the map of elevation difference for other glaciers in Norway (Langfjordjøkelen,
 Gråsubreen) because the patterns are highly similar.

352

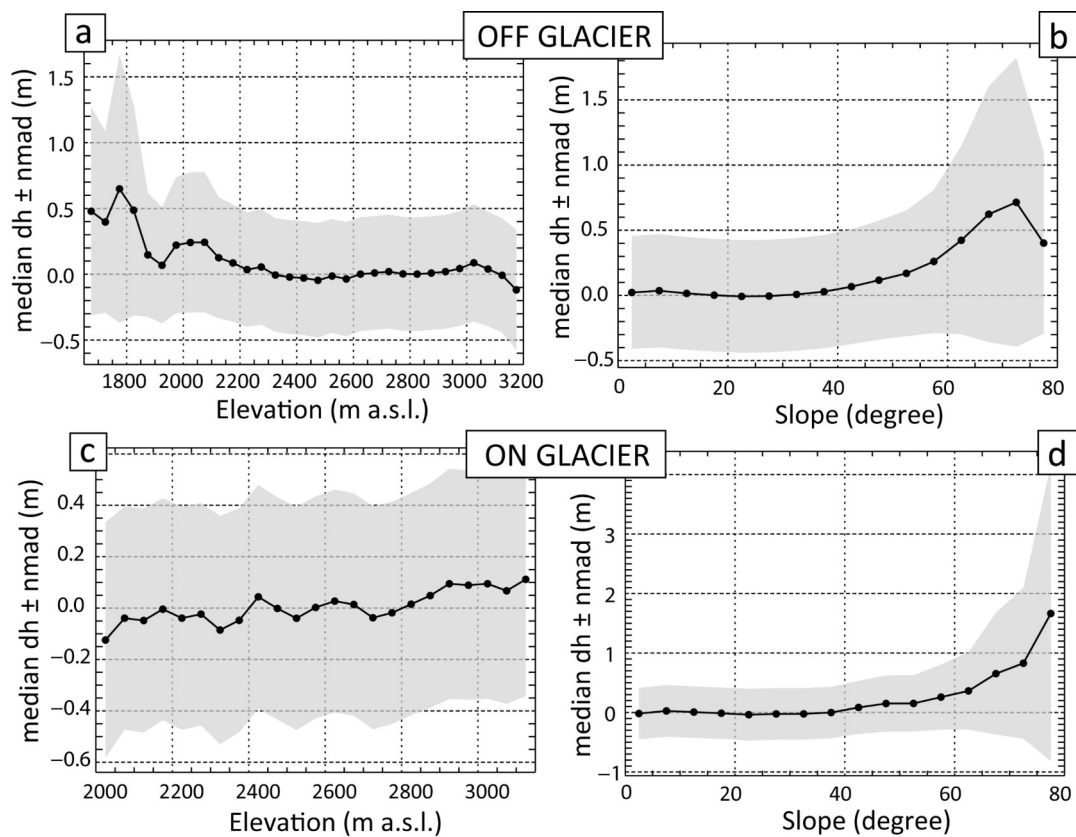
354 **Table 3. Statistics on the elevation differences (m) between the PGO 2 m DEMs and the Lidar DEMs acquired the**
 355 **same day. BM - Block matching. SGM - Semi-global matching. “Hellstugubreen” stands for “Hellstugubreen,**
 356 **Gråsubreen, Vestre Memurubreen, Austre Memurubreen”.**

	Median Dh off glac (m)	Median Dh on glac (m)	NMAD off glac (m)	NMAD on glac (m)
2016 Peyto - BM	0.02	-0.01	0.59	0.36
2016 Peyto - SGM	0.03	0.00	0.46	0.41
2018 Langfjordjøkelen - BM	0.01	-0.19	0.67	0.14
2018 Langfjordjøkelen - SGM	0.01	-0.14	0.54	0.17
2019 Hellstugubreen - BM	-0.01	-0.12	0.38	0.12
2019 Hellstugubreen - SGM	0.00	-0.09	0.29	0.15

358 As a result of the co-registration process~~By construction~~, the median elevation differences off glaciers
 359 are very close to 0 m. Over glacierized terrain, biases are also modest. Almost null for Peyto Glacier, they
 360 are slightly negative for the Norwegian sites but always within 0.2 m. Conversely, the dispersion of the
 361 residuals are slightly larger for the Canadian site, with a NMAD of about 0.4 m (a result of uncorrected
 362 jitter), while it ranges between 0.12 and 0.21 m for the glaciers in Norway. We note that the NMAD are
 363 systematically larger off glaciers than on glaciers which confirms that using the off glacier terrain to infer
 364 the uncertainty on glaciers is a conservative approach. Interestingly the choice of the correlation
 365 algorithm (BM or SGM) has a different influence on and off glaciers. SGM results in lower NMAD is
 366 superior off glaciers whereas using BM leads to reduced NMAD on glaciers.

The median elevation difference and its spread (quantified using the NMAD) are rather constant with
 368 elevation (Figure 87, only shown for the Peyto site, Canada). Off glacier, the positive elevation
 369 differences at low elevations are explained by the presence of vegetation (see also the southernmost
 370 portion of the map in Figure 7a-b). The Pléiades summer DEMs map the height of the canopy (Piermattei
 371 et al., 2019) while the lidar maps the bare ground below the vegetation (~~Piermattei et al., 2019~~). The bias
 372 and the NMAD are constant up to slopes of 50°. Above, the dispersion of the elevation difference
 373 increases rapidly (on and off glacier) and the median difference departs from 0. These results indicate
 374 that a good practice is to exclude areas of high reliefs (e.g., slopes larger than 50°) during coregistration
 375 and when computing the glacier-wide mean elevation changes.

376



378 **Figure 8. Median elevation differences (dh) between the Pléiades semi-global matching 2 m DEMs and the lidar**
 380 **DEM for the Peyto Glacier site (Canada). Median dh are plotted with elevation (left panels) and slope (right**
 382 **panels) off glaciers (upper panels) and on glaciers (lower panels). Points show median and shaded area shows**
NMAD of dh values (PGO DEM minus Lidar DEM) within each 50 m elevation bin (left) and each 5 degree
bin (right) off glaciers (upper panels) and on glaciers (lower panels). The grey shading corresponds to ± one
NMAD about the median.

384 Overall, these evaluations using lidar data suggest that glacier elevation changes can be measured from
 386 Pléiades DEMs with a sub-meter decimetric accuracy, with a minor influence of the processing
 388 algorithm. We note that these evaluations are performed on relatively small glaciers with abundant
 nearby stable terrain which is required for likely facilitate the coregistration and the bias corrections. So
 these results may not be readily transferable to larger glaciers.

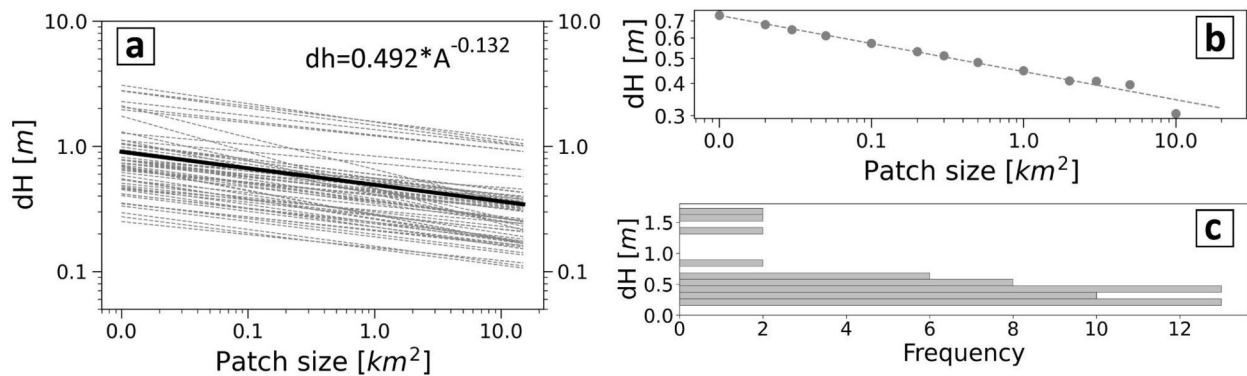
3.2. Uncertainty of the PGO glacier elevation changes

390 Uncertainties in the elevation difference from repeat Pléiades DEMs have previously been quantified
 392 with differential GNSS measurements with centimeter accuracy centimetric GNSS measurement. In the
 Mont Blanc massif, such measurements are repeated each year in early September along four transverse
 profiles on the Mer de Glace and on Argentière glaciers. For the 2021–22 mass balance year, the mean
 394 bias of the elevation difference was lower than 0.3 m and its standard deviation lower than 0.4 m
 (Berthier et al., in press). Similar values were found for elevation difference of Mera Glacier in Nepal
 396 from 2012 to 2018, with a mean bias of -0.24 m and standard deviation of 0.52 m (Wagnon et al., 2021).

Here, we quantified the uncertainty of the elevation changes systematically, taking advantage of
 398 the depth of the PGO archive. We used the elevation difference off glacier (as mapped in RGI v6.0) as a
 proxy of the uncertainty on glaciers, with the assumption that elevation difference should be 0 over
 400 “stable” terrain, and any observed residual is considered as error. This is a conservative choice as the

errors of the DEMs tend to increase with slope (Toutin, 2002; Lacroix, 2016; Hugonnet et al., 2022) and
 402 the average slopes are often gentler on glaciers than on nearby ice-free terrain (see also section 3.1.3).
 This is also conservative because during the five year time span separating the PGO DEMs, the off glacier
 404 terrain has evolved due to e.g., vegetation changes, destabilisation of recently deglaciated slopes. We
 calculated uncertainties (at the 95% confidence level) on the mean elevation change over a given area
 406 (ranging from 0.01 km² to 10 km²) using the patch method (Miles et al., 2018; Dussailant et al., 2018).
 For a given patch size, we extract the 95th percentile of the absolute mean elevation difference. We
 408 analysed 58 PGO elevation difference maps for which the off glacier terrain covered at least 50 km²
 (Figure 9).

410



412 **Figure 9. (a) Uncertainties (dh) at the 95% confidence level (2-sigma) for 58 PGO maps of elevation changes as a**
function of the averaging area. The dashed lines correspond to individual maps of elevation changes obtained
 414 **from the 2-m BM DEMs and for which the stable terrain occupies more than 50 km². The thick black line**
corresponds to the mean of all these individual lines and its equation is provided. (b) Example of the uncertainty
 416 **(at the 95% confidence interval) as a function of the patch size for one of the PGO repeat surveys on**
Langfjordjokelen in Norway. (c) Distribution of the uncertainties for the 58 elevation difference maps and a patch
 418 **size of 1 km².**

420 [] We observe a relatively large spread of the uncertainties on the elevation differences despite the fact
 that they are all derived from repeat Pléiades DEMs. For example, the 2-sigma uncertainties for a 1 km²
 patch size range from 0.15 m up to 1.5 m. The largest uncertainties (between 1.2 and 1.5 m, n=6)
 422 correspond to maps of elevation difference affected by a larger jitter in the Pléiades DEMs and only
 partly corrected by our along-track spline correction. This is for example the case for the Tuyuksu
 424 (Central Asia) 2016–2021 elevation difference maps shown in Figure 4. Excluding these anomalous
peculiar six maps, the remaining uncertainties (95% confidence level) are on average 0.38 m for a 1 km²
 426 patch size with a limited spread (n=52, min=0.15 m, max=0.83 m, standard deviation = 0.15 m). The
 variance of the mean slope off glacier only explains a small fraction (13%) of the variance in these
 428 uncertainties. These mean uncertainties are in agreement with the one derived from same-day lidar
 surveys (section 3.1.3).

430

4. Are PGO sites representative of the Earth's glaciers?

432 [] The ASTER VNIR sensor, on board the TERRA platform, is the only sensorsatellite mission in orbit
 providing publicly-available global coverage using optical stereoscopic images. Recently, it was used to

434 generate maps of elevation changes and hence to calculate glacier-wide mass balances for almost all the
Earth's glaciers from 2000 to 2019 (Hugonnet et al., 2021). However, ASTER will stop acquiring images in
436 2026⁵ (or 2027⁶) and no satellite mission is scheduled to provide publicly-available, global coverage with
| stereo images. Very high resolution sensors like Pléiades are not fully dedicated to science applications
438 and, currently, do not have the capability to replace ASTER. It is useful, however, to assess whether the
| 140 glacier sites surveyed by the PGO provide a reasonable assessment of global glacier mass change ~~for~~
440 Earth's glaciated environments.

To determine the representativeness of the PGO sampling, we extracted from the Hugonnet et
442 al. (2021) database, the glacier-wide mass balance of glaciers intersecting the PGO sites (named
hereafter 'PGO glaciers'). For glaciers only partly covered in a PGO site, we retained those with at least
444 50% coverage. There are about 6800 PGO glaciers and, in area, they cover 2.5% of the world's glaciers
(Table 3). By region, the coverage is highly heterogeneous and varies from 0% in the Russian Arctic to
446 almost 47% in New Zealand. We clarify here that, in this entire analysis, none of the mass balances were
| derived from PGO elevation change maps. All mass balances are from the Hugonnet et al. (2021)
448 database.

[] For each GTN-G first order glacier region, we then computed the region-wide mass balances as the
450 area-weighted sum of the PGO glacier-wide mass balances and compared these regionally-aggregated
| values with corresponding values using the full sample from Hugonnet et al. (2021) to the Hugonnet et al.
452 (2021)'s values, using the full sample of glaciers. Three periods were considered, 2000–2019, i.e. the full
period for which the uncertainties are the smallest in Hugonnet et al. database and also two sub-periods,
454 2000–09 and 2010–19, to test the ability of PGO glaciers to capture the change in mass balance from one
decade to another (Figure 10).

456 [] At global scale, excluding the unsampled Russian Arctic, the global mass balance during 2000–19 was
–0.39±0.02 w.e./yr (Hugonnet et al., 2021). Using only the values for PGO glaciers (Table 4), the global
458 mass balance is slightly more negative (–0.46 m w.e./yr). PGO glaciers capture rather well the
acceleration of the mass loss that occurred from 2000–09 to 2010–19. The full sample indicates a drop
460 of the mass balance by 0.05 m w.e./yr between the two periods, PGO glaciers see an almost identical
drop of 0.07 m w.e./yr.

462 At the scale of the 18 individual GTN-G first order regions (Figure 10, Table 4, Russian Arctic
excluded), the mass balance differences between the full sample and PGO glaciers are larger. When the
464 20-yr period is considered, the differences in region-wide mass balance can be as large as 0.34 m w.e./yr
(region: Iceland) with a standard deviation of 0.16 m w.e./yr (n=18). Again, PGO glaciers perform better
466 at capturing the change in mass balance between the two 10-yr periods: the maximum difference is 0.21
m w.e./yr (region: Western Canada and USA) and the minimum difference is –0.15 m w.e./yr (regions:
468 South Asia West and Subantarctic and Antarctic Islands), the standard deviation being 0.09 m w.e./yr.
For 10 out of 18 RGI regions, the change in region-wide mass balance is observed by PGO glaciers with
470 an error of less than 0.05 m w.e./yr.

[] Hence, even if the PGO sites were not chosen to represent the World's glaciers, they still provide a
472 reasonable estimate of their mass balance and this sample is able to perform even better at capturing
their temporal changes. Yet, one strong complication to use these glaciers for a global mass change
474 analysis would be related to the fact that the Pléiades acquisitions on the 140 PGO glacier sites are not
performed simultaneously but using a moving temporal window (Table 1).

476 It should be noted that there are uncertainties in the Hugonnet et al. (2021) data and that they
 are not necessarily representative for smaller samples of glaciers or shorter periods (e.g., Andreassen et
 478 al., 2023; Berthier et al., 2023). At local scale and for periods of a few months or years, repeated lidar or
 other high resolution DEMs (e.g. PGO) give more accurate results.

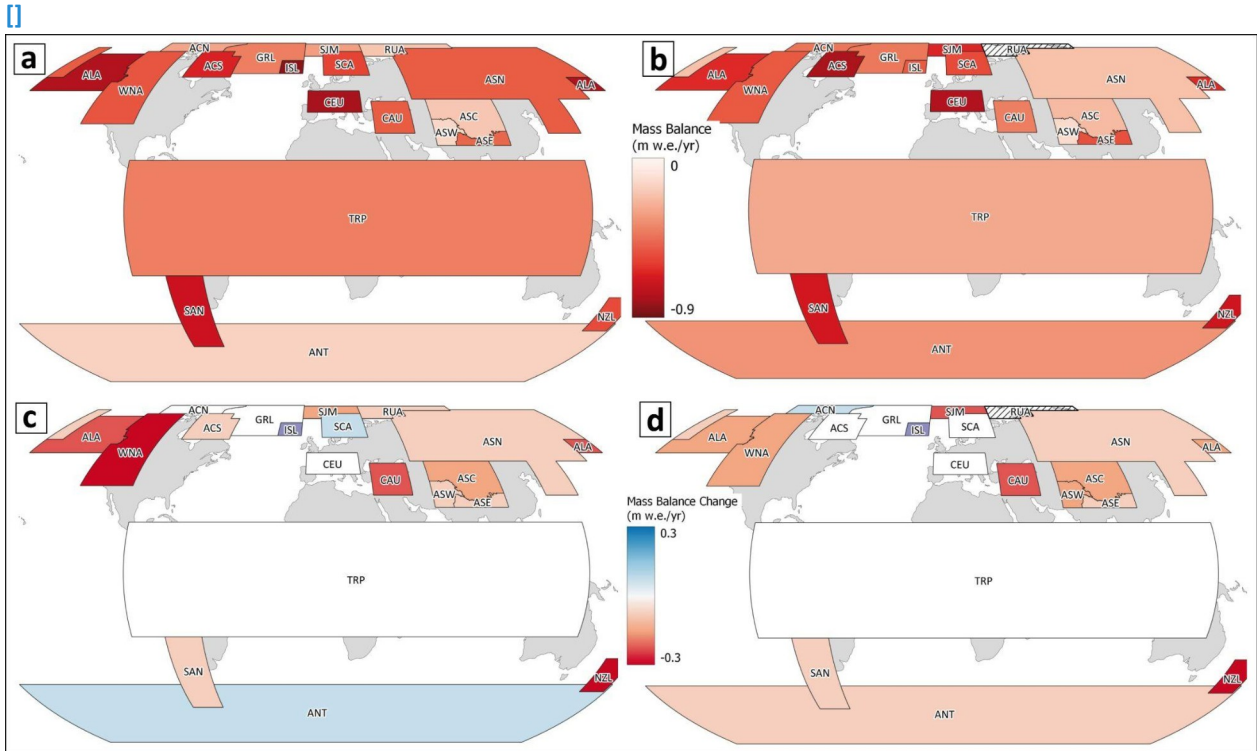
480

482 **Table 3. Fraction of the Earth’s glacier sampled by the PGO. The number and area of glaciers refer to the**
RGI v6.0 inventory except in region 12 (Caucasus and Middle East) where the Global Land Ice Measurements
 484 **from Space (GLIMS) outlines are used, as in Hugonnet et al. (2021).**

	GTN-G region	Number of glaciers	Glacier area km ²	Number of PGO sites	Number of PGO glaciers*	Area of PGO glaciers (in % of the total)
1	Alaska	27,108	86,725	6	190	1.0
2	Western Canada and USA	18,855	14,524	5	268	3.5
3	Arctic Canada North	4556	105,111	4	22	0.4
4	Arctic Canada South	7415	40,888	2	54	0.8
5	Greenland Periphery	19,306	89,717	8	255	1.9
6	Iceland	568	11060	1	17	1.6
7	Svalbard and Jan Mayen	1615	34187	6	60	3.2
8	Scandinavia	3417	2949	5	238	17.3
9	Russian Arctic	1069	51,592	0	0	0
10	North Asia	5151	2410	2	113	7.1
11	Central Europe	3927	2092	13	882	33.3
12	Caucasus and Middle East	3516	1336	3	344	25.8
13	Central Asia	54,429	49,303	12	1185	4.5
14	South Asia West	27,988	33,568	5	301	1.7
15	South Asia East	13,119	14,734	9	624	7.9
16	Low Latitudes	2939	2341	9	220	12.6
17	Southern Andes	15,908	29,429	30	894	10.3
18	New Zealand	3537	1162	6	935	46.8
19	Subantarctic and Antarctic Islands	2752	132,867	14	208	2.2
	Global	217,715	705,995	140	6810	2.5
	Global excl. Russian Arctic	216,106	654,405	140	6810	2.7

* We only count glaciers for which at least 50% of the area is covered.

486



488

Figure 10. Comparison of the 2000-2019 region-wide mass balances calculated using the entire Hugonnet et al. (2021)'s dataset (a) and using only the glaciers sampled by the PGO (b). The lower panels show the changes in region-wide mass balances between 2000-2009 and 2010-2019 for (c) all glaciers and for (d) the subset of glaciers sampled by the PGO. **All mass balances are from the Hugonnet et al. (2021) database (i.e., none were derived from PGO elevation change maps).**

494 **Table 4. Regional and global mass balances (in m w.e./yr) from the entire RGI sample (Hugonnet et al., 2021)**
 496 **and from the PGO glaciers (this study). MB stands for mass balance. Delta_MB corresponds to the change in**
region-wide mass balance from 2000–09 to 2010–19. All mass balances are from the Hugonnet et al. (2021)
database (i.e. none were derived from PGO elevation change maps).

	GTN-G region	MB 2000-19 ALL	MB 2000-19 PGO	Delta_MB ALL	Delta_MB PGO
1	Alaska	-0.77	-0.63	0.12	0.16
2	Western Canada and USA	-0.52	-0.51	-0.10	0.11
3	Arctic Canada North	-0.29	-0.43	-0.18	-0.09
4	Arctic Canada South	-0.65	-0.79	-0.21	-0.06
5	Greenland Periphery	-0.40	-0.42	0.00	-0.04
6	Iceland	-0.85	-0.51	0.36	0.32
7	Svalbard and Jan Mayen	-0.31	-0.64	-0.28	-0.39
8	Scandinavia	-0.57	-0.55	0.05	-0.01
9	Russian Arctic	-0.20	NaN	-0.06	NaN
10	North Asia	-0.50	-0.21	0.28	0.31
11	Central Europe	-0.80	-0.77	0.05	0.00
12	Caucasus and Middle East	-0.50	-0.40	0.08	0.12
13	Central Asia	-0.19	-0.23	-0.02	-0.05
14	South Asia West	-0.14	-0.13	0.08	-0.07
15	South Asia East	-0.47	-0.53	-0.05	-0.08
16	Low Latitudes	-0.40	-0.28	0.12	0.10
17	Southern Andes	-0.70	-0.68	0.02	0.01
18	New Zealand	-0.55	-0.69	-0.10	-0.18
19	Subantarctic and Antarctic Islands	-0.16	-0.34	-0.10	-0.25
	Global excl. Russian Arctic	-0.39	-0.46	-0.05	-0.07

498

5. Conclusion

500 The Pléiades Glacier Observatory is an initiative by the French Space Agency (CNES) and LEGOS to
 502 facilitate access to very high resolution digital elevation models, [elevation change maps](#), and, after
 signing a licence, ortho-images of glaciers. Such data are useful to calculate glacier geodetic mass
 balances, but also to support other glaciology oriented applications, such as updating glacier outlines,
 504 extracting glacier hypsometry or qualitatively documenting glacier changes. The PGO aims at managing
 the Pléiades acquisitions, and distributing products that are tailored for glaciological applications, and as
 506 user friendly as possible. The acquisitions started in 2016 and during the first five years, acquired stereo-
 pairs over 140 target sites around the globe, selected through a call to the glaciological community.
 508 Since 2021, these acquisitions have been progressively repeated to produce maps of elevation change
 over five years. At the time of writing, already 31 publications used PGO data to examine glacier

510 changes.

512 | We quantified the uncertainties of the DEMs (after coregistration to the Copernicus GLO-30 DEM) and
514 | elevation change maps derived from repeat Pléiades DEMs. This was done with two methods: (1)
516 | comparison to near-contemporaneous simultaneous accurate lidar surveys, and (2) using the stable-
518 | terrain as a proxy of the uncertainties on glaciers residual elevation difference values on nearby stable
516 | terrain to estimate corresponding uncertainty on glacier surfaces. Both methods agree broadly on the
518 | uncertainties, and as a rule of thumb, the mean glacier-wide elevation differences have a 2-sigma
518 | uncertainty of about 0.5 m for a glacier of 1 km² or larger. ~~While these uncertainties characterise the~~
518 | ~~area-averaged elevation change between two Pléiades DEM, other sources of error exist for geodetic-~~
518 | ~~mass balance such as uncertainties in glacier area and on the volume to mass conversion factor.~~

520 Pléiades satellites are planned to orbit until 2026. Access to data from their successors (Pléiades Neo) is
522 | not yet secured for the scientific community and the cost may be prohibitive. It should be a priority for
522 | the space agencies to continue to provide high resolution stereo-imagery to scientists to observe the
522 | imprint of climate change on the Earth surface and in particular on glaciers.

524 **Data availability statement**

526 | Pléiades Glacier Observatory DEMs and elevation change products are under CC-BY-NC licence and freely
526 | available at: <https://a2s-dissemination.u-strasbg.fr/#!>

528 | Licensing issues prevent ~~us from~~ openly distribution of primary distributing the Pléiades products and
528 | ortho-images. These imagesy are available after signing the Pléiades institutional scientific licence to be
528 | requested to the French space agency CNES (dinamis@cnes.fr).

530 | ~~At the time of submission, the elevation change products cannot be accessed yet on a map server. They~~
532 | ~~are available upon request to the corresponding author. As soon as a distribution platform is~~
532 | ~~operational, data availability will be advertised on the PGO website (<https://www.legos.omp.eu/pgo/>).~~

534 | The scripts used to generate the DEMs and ortho-images and to coregister them to GLO-30 are available
534 | at: <https://zenodo.org/uploads/12909586> upon request to the corresponding author.

Author contributions

536 | EB designed the PGO program with contribution from DF and SH. JL and EB generated the DEMs and
536 | elevation change maps. JMCB, LMA and BM provided Lidar data and all related analysis. ~~DF and SH~~
538 | ~~helped with the project design and the image acquisitions. All authors contributed to the discussion of~~
538 | ~~the results.~~ CB worked on the regional representativity of the PGO sites. All authors contributed to the
540 | discussion of the results. EB prepared the manuscript with contributions from all co-authors.

Competing interests

542 | One author (EB) is a member of the editorial board of The Cryosphere.

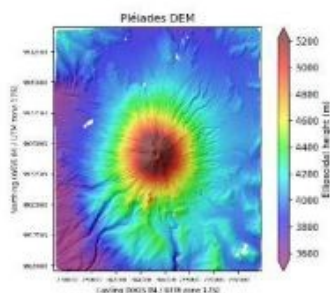
Acknowledgments

544 | E. Berthier and J. Lebreton acknowledge support from the French Space Agency (CNES). B.
544 | Menounos acknowledges funding from the Natural Sciences and Engineering Research Council
546 | of Canada and the Tula Foundation. L.M. Andreassen acknowledges the internal NVE project
546 | ‘N80524 Regionalt massebalanseestimat av norske breer’. This is also a contribution to the

548 International Association of Cryospheric Sciences (IACS) working group on Regional Assessments of Glacier Mass Change (RAGMAC).

550

Appendix



Pléiades Glacier Observatory : DEM

Date : 2016-11-15
Site : Cotopaxi_TRP

DEM information

Coordinate system	UTM 17 south - EPSG 32717
Correlation algorithm	Semi Global Matching (SGM)
DEM resolution	2 m and 20 m
Reference for height	Ellipsoidal Height (WGS84)
Shift vector to Copernicus GLO-30 (m)	dx=-2.69; dy=-2.64; dz=+1.74
Base-to-Height ratio (B/H)	0.42

Source images

PHR DS_PHR1B_201611151534305_FR1_PX_W079S01_0708_01575
PHR DS_PHR1B_201611151535093_FR1_PX_W079S01_0708_01604

Copyright

Pléiades © CNES Year_of_acquisition, Distribution Airbus D&S

Archive structure

```
└─ 2016-11-15_1535065_Cotopaxi_TRP
  └─ BM
    ├── 2016-11-15_1535065_Cotopaxi_TRP_footprint.shp
    ├── 2016-11-15_1535065_Cotopaxi_TRP_footprint.dbf
    ├── 2016-11-15_1535065_Cotopaxi_TRP_footprint.prj
    └── 2016-11-15_1535065_Cotopaxi_TRP_footprint.shx
  └─ SGM
    ├── 2016-11-15_1535065_Cotopaxi_TRP_1B_DEM_SGM_2m.tif
    ├── 2016-11-15_1535065_Cotopaxi_TRP_1B_DEM_SGM_20m.tif
    ├── README_SGM_DEM.pdf
    ├── PREVIEW_2016-11-15_1535065_Cotopaxi_TRP_1B_DEM_SGM_20m.png
    └── Coreg_2016-11-15_1535065_Cotopaxi_TRP_1B_DEM_SGM_20m_vs_Cop30.png
```

Description

DEMs and orthoimages were generated from raw Pléiades images using the Ames Stereo Pipeline [Beyer et al., 2018]. The set of processing parameters used for DEM generation are from [Marti et al., TC, 2016] for block matching -BM- and from [Deschamps-Berger et al., 2020] for semi global matching -SGM.

All DEMs and orthoimages are coregistered on the Copernicus GLO-30 DEM using the demcoreg tool [Shean et al., 2021].

Acknowledgement statement: The Pléiades images/DEMs used in this study was provided by the Pléiades Glacier Observatory initiative of the French Space Agency (CNES) and Laboratoire d'Etudes en Géophysique et Océanographie Spatiales (LEGOS).

When an image is shown in a presentation, website or an article, the copyright should be (Pléiades © CNES Year_of_acquisition, Distribution Airbus D&S).

We remind to cope with the licence rules regarding (no) data sharing and no commercial use.

References

Beyer et al.: The Ames Stereo Pipeline: NASA's Open Source Software for Deriving and Processing Terrain Data, Earth and Space Science, 5(9), 537–548, doi:10.1029/2018EA000409, 2018.

Shean et al.: dshean/demcoreg, Zenodo, v1.1.0, <https://doi.org/10.5281/zenodo.5733347>, 2021.

Deschamps-Berger et al.: Snow depth mapping from stereo satellite imagery in mountainous terrain: evaluation using airborne laser-scanning data, The Cryosphere, 14(9), 2925–2940, <https://doi.org/10.5194/tc-14-2925-2020>, 2020.

Marti et al.: Mapping snow depth in open alpine terrain from stereo satellite imagery, The Cryosphere, 10(4), 1361–1380, doi:10.5194/tc-10-1361-2016, 2016.

552

pendix **Figure A1**: Example of the fact sheet accompanying each PGO product, here the semi-global matching (SGM) DEMs over the Cotopaxi area acquired 15 November 2016.

554

Ap

556 **Appendix Table A1: The 140 sites of the Pléiades Glacier Observatory. The list is ordered chronologically by**
558 **campaign (HN for North Hemisphere, HS for South Hemisphere). The name of each site is followed by the 3**
letters of the GTN-G first order region it belongs to. The table also lists the latitude, longitude of each site, the
number of TDI stages that were used during the image acquisitions and the number of stereo pairs needed to
cover the entire site.

560

<u>Campaign</u>	<u>Site_Region</u>	<u>Latitude</u> (°)	<u>Longitude</u> (°)	<u>Nb TDI</u> <u>stages</u>	<u>Nb stereo pairs</u>
<u>2016_HN</u>	<u>Antisana_TRP</u>	<u>0</u>	<u>-78</u>	<u>10</u>	<u>1</u>
<u>2016_HN</u>	<u>Bologna_WNA</u>	<u>62</u>	<u>-128</u>	<u>10</u>	<u>3</u>
<u>2016_HN</u>	<u>Broggerhalvoya_SJM</u>	<u>78.7</u>	<u>12.6</u>	<u>13</u>	<u>3</u>
<u>2016_HN</u>	<u>Columbia_WNA</u>	<u>52</u>	<u>-117.5</u>	<u>10</u>	<u>2</u>
<u>2016_HN</u>	<u>Cotopaxi_TRP</u>	<u>-0.7</u>	<u>-78.43</u>	<u>10</u>	<u>1</u>
<u>2016_HN</u>	<u>Garibaldi_WNA</u>	<u>50</u>	<u>-123</u>	<u>10</u>	<u>2</u>
<u>2016_HN</u>	<u>Grisefiord_ACN</u>	<u>76.5</u>	<u>-82.5</u>	<u>13</u>	<u>2</u>
<u>2016_HN</u>	<u>Gulkana_ALA</u>	<u>63.5</u>	<u>-145.5</u>	<u>10</u>	<u>2</u>
<u>2016_HN</u>	<u>Kongsfjord_SJM</u>	<u>79</u>	<u>12.6</u>	<u>13</u>	<u>2</u>
<u>2016_HN</u>	<u>Meighen_ACN</u>	<u>80</u>	<u>-99.5</u>	<u>13</u>	<u>1</u>
<u>2016_HN</u>	<u>Melville_ACN</u>	<u>75.5</u>	<u>-115</u>	<u>13</u>	<u>1</u>
<u>2016_HN</u>	<u>Ortles_CUE</u>	<u>46.5</u>	<u>10.5</u>	<u>10</u>	<u>2</u>
<u>2016_HN</u>	<u>Sonnblickkees_CUE</u>	<u>47</u>	<u>12.5</u>	<u>10</u>	<u>2</u>
<u>2016_HN</u>	<u>Svetisen_SCA</u>	<u>66.5</u>	<u>14</u>	<u>10</u>	<u>1</u>
<u>2016_HN</u>	<u>Tuyuksu_ASC</u>	<u>43</u>	<u>77</u>	<u>10</u>	<u>2</u>
<u>2016_HN</u>	<u>Wapta_WNA</u>	<u>51.5</u>	<u>-116.5</u>	<u>10</u>	<u>1</u>
<u>2016_HN</u>	<u>Wolverine_ALA</u>	<u>60.5</u>	<u>-149</u>	<u>10</u>	<u>1</u>
<u>2016_HN</u>	<u>Yasghil_ASW</u>	<u>36.5</u>	<u>75.5</u>	<u>10</u>	<u>1</u>
<u>2017_HS</u>	<u>Alvear_SAN</u>	<u>-55</u>	<u>-68</u>	<u>10</u>	<u>1</u>
<u>2017_HS</u>	<u>BahiaDelDiablo_ANT</u>	<u>-63.75</u>	<u>-67.5</u>	<u>13</u>	<u>2</u>
<u>2017_HS</u>	<u>GardenEden_NZL</u>	<u>-43.25</u>	<u>170.75</u>	<u>10</u>	<u>4</u>
<u>2017_HS</u>	<u>Gourdon_ANT</u>	<u>-64.25</u>	<u>-67.5</u>	<u>13</u>	<u>2</u>
<u>2017_HS</u>	<u>Hudson_SAN</u>	<u>-46</u>	<u>-73</u>	<u>10</u>	<u>2</u>
<u>2017_HS</u>	<u>Lautaro_SAN</u>	<u>-49</u>	<u>-73.5</u>	<u>10</u>	<u>2</u>
<u>2017_HS</u>	<u>MtAspiring_NZL</u>	<u>-44.5</u>	<u>168.5</u>	<u>10</u>	<u>3</u>
<u>2017_HS</u>	<u>MtCook_NZL</u>	<u>-43.5</u>	<u>170.25</u>	<u>10</u>	<u>3</u>
<u>2017_HS</u>	<u>Olivares_SAN</u>	<u>-33</u>	<u>-70</u>	<u>10</u>	<u>2</u>
<u>2017_HS</u>	<u>Peteroa_SAN</u>	<u>-35.5</u>	<u>-70.5</u>	<u>10</u>	<u>1</u>
<u>2017_HS</u>	<u>RioToro_SAN</u>	<u>-49</u>	<u>-73</u>	<u>10</u>	<u>1</u>
<u>2017_HS</u>	<u>SierraBeauvoir_SAN</u>	<u>-54</u>	<u>-68.5</u>	<u>10</u>	<u>3</u>
<u>2017_HS</u>	<u>Tronador_SAN</u>	<u>-41.15</u>	<u>-71.9</u>	<u>10</u>	<u>1</u>
<u>2017_HS</u>	<u>Ushuaia_SAN</u>	<u>-55</u>	<u>-68.5</u>	<u>10</u>	<u>1</u>
<u>2017_HN</u>	<u>Elbrus_CAU</u>	<u>43.25</u>	<u>42.5</u>	<u>10</u>	<u>1</u>
<u>2017_HN</u>	<u>Fedchenko_ASC</u>	<u>38.75</u>	<u>72.15</u>	<u>10</u>	<u>6</u>
<u>2017_HN</u>	<u>GranParadis_CEU</u>	<u>45.5</u>	<u>7</u>	<u>10</u>	<u>2</u>
<u>2017_HN</u>	<u>Hansbreen_SJM</u>	<u>77</u>	<u>15.5</u>	<u>13</u>	<u>1</u>
<u>2017_HN</u>	<u>Hornbreen_SJM</u>	<u>77</u>	<u>17</u>	<u>13</u>	<u>1</u>
<u>2017_HN</u>	<u>Kaffioyra_SJM</u>	<u>78.5</u>	<u>12.5</u>	<u>13</u>	<u>1</u>
<u>2017_HN</u>	<u>Kaunertal_CEU</u>	<u>47</u>	<u>10.75</u>	<u>10</u>	<u>2</u>
<u>2017_HN</u>	<u>Langfjordjokelen_SCA</u>	<u>70</u>	<u>22</u>	<u>13</u>	<u>2</u>
<u>2017_HN</u>	<u>Langtang_ASE</u>	<u>28.25</u>	<u>85.7</u>	<u>10</u>	<u>2</u>
<u>2017_HN</u>	<u>Lingmarksbraeen_GRL</u>	<u>69.25</u>	<u>-53.5</u>	<u>13</u>	<u>1</u>
<u>2017_HN</u>	<u>Lombardy_CEU</u>	<u>46.25</u>	<u>10</u>	<u>10</u>	<u>2</u>
<u>2017_HN</u>	<u>Lunana_ASE</u>	<u>28</u>	<u>90.25</u>	<u>10</u>	<u>2</u>
<u>2017_HN</u>	<u>Olsen_GRL</u>	<u>74.75</u>	<u>-22</u>	<u>13</u>	<u>2</u>
<u>2017_HN</u>	<u>Oraefajokull_ISL</u>	<u>64</u>	<u>-16.5</u>	<u>13</u>	<u>2</u>
<u>2017_HN</u>	<u>Pasterze_CEU</u>	<u>47</u>	<u>12.75</u>	<u>10</u>	<u>2</u>
<u>2017_HN</u>	<u>Qaanaaq_GRL</u>	<u>77.5</u>	<u>-69.5</u>	<u>13</u>	<u>2</u>

<u>2017 HN</u>	<u>Qasigiannguit GRL</u>	<u>64</u>	<u>-51</u>	<u>13</u>	<u>2</u>
<u>2017 HN</u>	<u>QuelccayalceCap TRP</u>	<u>-14</u>	<u>-70.75</u>	<u>10</u>	<u>2</u>
<u>2017 HN</u>	<u>RedRockCliff GRL</u>	<u>77</u>	<u>-67.5</u>	<u>13</u>	<u>1</u>
<u>2017 HN</u>	<u>Rhone CEU</u>	<u>46.5</u>	<u>8.5</u>	<u>10</u>	<u>2</u>
<u>2017 HN</u>	<u>RikhaSamba ASE</u>	<u>28.75</u>	<u>83.5</u>	<u>10</u>	<u>1</u>
<u>2017 HN</u>	<u>Sarek SCA</u>	<u>77</u>	<u>17.5</u>	<u>13</u>	<u>2</u>
<u>2017 HN</u>	<u>Silvretta CEU</u>	<u>47</u>	<u>10</u>	<u>10</u>	<u>1</u>
<u>2017 HN</u>	<u>Stubai CEU</u>	<u>47</u>	<u>11</u>	<u>10</u>	<u>2</u>
<u>2017 HN</u>	<u>Trambau ASE</u>	<u>28</u>	<u>86.5</u>	<u>10</u>	<u>2</u>
<u>2017 HN</u>	<u>Valpelline CEU</u>	<u>45.5</u>	<u>7</u>	<u>10</u>	<u>2</u>
<u>2017 HN</u>	<u>Variigated ALA</u>	<u>60</u>	<u>-139.2</u>	<u>10</u>	<u>3</u>
<u>2017 HN</u>	<u>Venediger CEU</u>	<u>47</u>	<u>12.75</u>	<u>10</u>	<u>1</u>
<u>2017 HN</u>	<u>Zillertal CEU</u>	<u>47</u>	<u>11.75</u>	<u>10</u>	<u>1</u>
<u>2018 HS</u>	<u>Chico SAN</u>	<u>-49</u>	<u>-73</u>	<u>10</u>	<u>5</u>
<u>2018 HS</u>	<u>Cocuy TRP</u>	<u>6.5</u>	<u>-72.25</u>	<u>10</u>	<u>1</u>
<u>2018 HS</u>	<u>Grey SAN</u>	<u>-51</u>	<u>-73.5</u>	<u>10</u>	<u>4</u>
<u>2018 HS</u>	<u>Huascaran TRP</u>	<u>-9.05</u>	<u>-77.6</u>	<u>10</u>	<u>1</u>
<u>2018 HS</u>	<u>PeritoMoreno SAN</u>	<u>-50.5</u>	<u>-73</u>	<u>10</u>	<u>3</u>
<u>2018 HS</u>	<u>Rolleston NZL</u>	<u>-43</u>	<u>171.5</u>	<u>10</u>	<u>1</u>
<u>2018 HS</u>	<u>SanLorenzo SAN</u>	<u>-47.5</u>	<u>-72.25</u>	<u>10</u>	<u>2</u>
<u>2018 HS</u>	<u>SantaMarta TRP</u>	<u>10.84</u>	<u>-73.7</u>	<u>10</u>	<u>2</u>
<u>2018 HS</u>	<u>Tupungato SAN</u>	<u>-33.5</u>	<u>-69.75</u>	<u>10</u>	<u>3</u>
<u>2018 HN</u>	<u>AruCo ASC</u>	<u>34</u>	<u>82.25</u>	<u>10</u>	<u>1</u>
<u>2018 HN</u>	<u>BashKhaindy ASC</u>	<u>41</u>	<u>76</u>	<u>10</u>	<u>2</u>
<u>2018 HN</u>	<u>Dachstein CEU</u>	<u>47.5</u>	<u>13.5</u>	<u>10</u>	<u>1</u>
<u>2018 HN</u>	<u>Karabatkak ASC</u>	<u>42</u>	<u>78.25</u>	<u>10</u>	<u>1</u>
<u>2018 HN</u>	<u>Kketau ASC</u>	<u>45</u>	<u>80.5</u>	<u>10</u>	<u>1</u>
<u>2018 HN</u>	<u>Konsvegen SJM</u>	<u>78.75</u>	<u>13</u>	<u>10</u>	<u>2</u>
<u>2018 HN</u>	<u>LemonCreek ALA</u>	<u>58.5</u>	<u>-134.5</u>	<u>10</u>	<u>1</u>
<u>2018 HN</u>	<u>Makalu ASE</u>	<u>27.75</u>	<u>87</u>	<u>10</u>	<u>2</u>
<u>2018 HN</u>	<u>Mittivakkat GRL</u>	<u>65.75</u>	<u>-35.5</u>	<u>10</u>	<u>3</u>
<u>2018 HN</u>	<u>Purogangri ASC</u>	<u>34</u>	<u>89</u>	<u>10</u>	<u>3</u>
<u>2018 HN</u>	<u>Satopanth ASE</u>	<u>30.75</u>	<u>79.5</u>	<u>10</u>	<u>4</u>
<u>2018 HN</u>	<u>Thana ASE</u>	<u>28</u>	<u>90.75</u>	<u>10</u>	<u>2</u>
<u>2018 HN</u>	<u>White ACN</u>	<u>79.5</u>	<u>-91</u>	<u>13</u>	<u>2</u>
<u>2019 HS</u>	<u>AguaNegra SAN</u>	<u>-30.25</u>	<u>-69.75</u>	<u>10</u>	<u>3</u>
<u>2019 HS</u>	<u>Heard ANT</u>	<u>-53</u>	<u>73.5</u>	<u>10</u>	<u>4</u>
<u>2019 HS</u>	<u>Livingstone ANT</u>	<u>-62.5</u>	<u>-60.5</u>	<u>13</u>	<u>9</u>
<u>2019 HS</u>	<u>SanQuintin SAN</u>	<u>-47</u>	<u>-73.75</u>	<u>10</u>	<u>6</u>
<u>2019 HS</u>	<u>Universidad SAN</u>	<u>-34.5</u>	<u>-70.25</u>	<u>10</u>	<u>1</u>
<u>2019 HN</u>	<u>Aktru ASN</u>	<u>50</u>	<u>87.5</u>	<u>10</u>	<u>2</u>
<u>2019 HN</u>	<u>Aqqutikitsoq GRL</u>	<u>67.15</u>	<u>-53</u>	<u>10</u>	<u>3</u>
<u>2019 HN</u>	<u>Barkrak ASC</u>	<u>42.15</u>	<u>71</u>	<u>10</u>	<u>3</u>
<u>2019 HN</u>	<u>Bezengi CAU</u>	<u>43</u>	<u>43.2</u>	<u>10</u>	<u>2</u>
<u>2019 HN</u>	<u>DeLongIslands ASN</u>	<u>76.75</u>	<u>148.75</u>	<u>13</u>	<u>2</u>
<u>2019 HN</u>	<u>Grinnell ACS</u>	<u>62.6</u>	<u>-66.75</u>	<u>10</u>	<u>1</u>
<u>2019 HN</u>	<u>HolmLand GRL</u>	<u>80.35</u>	<u>-17</u>	<u>10</u>	<u>10</u>
<u>2019 HN</u>	<u>Jotunheinmen SCA</u>	<u>61.5</u>	<u>8.5</u>	<u>10</u>	<u>3</u>
<u>2019 HN</u>	<u>Kilimanjaro TRP</u>	<u>-3</u>	<u>37.5</u>	<u>10</u>	<u>1</u>
<u>2019 HN</u>	<u>Kolka CAU</u>	<u>42.75</u>	<u>44.5</u>	<u>10</u>	<u>2</u>
<u>2019 HN</u>	<u>Parlung24K ASE</u>	<u>29.75</u>	<u>95.75</u>	<u>10</u>	<u>2</u>
<u>2019 HN</u>	<u>ParlungN4 ASE</u>	<u>29</u>	<u>97</u>	<u>10</u>	<u>2</u>
<u>2019 HN</u>	<u>TerraNivae ACS</u>	<u>62.3</u>	<u>-66.5</u>	<u>10</u>	<u>2</u>
<u>2019 HN</u>	<u>Zulmart ASC</u>	<u>38.85</u>	<u>73</u>	<u>10</u>	<u>1</u>
<u>2020 HS</u>	<u>DaviesDome ANT</u>	<u>-64</u>	<u>-58</u>	<u>10</u>	<u>2</u>
<u>2020 HS</u>	<u>Domuyo SAN</u>	<u>-36.6</u>	<u>-70.4</u>	<u>10</u>	<u>1</u>

<u>2020_HS</u>	<u>EsteroDerecho_SAN</u>	<u>-30.4</u>	<u>-70.4</u>	<u>10</u>	<u>2</u>
<u>2020_HS</u>	<u>Fiordland_NZL</u>	<u>-44.7</u>	<u>168</u>	<u>10</u>	<u>2</u>
<u>2020_HS</u>	<u>GlaciarDeLosTres_SAN</u>	<u>-49.3</u>	<u>-73</u>	<u>10</u>	<u>1</u>
	<u>GranCampoNevado_SA</u>	<u>-52.75</u>	<u>-73</u>	<u>10</u>	<u>2</u>
<u>2020_HS</u>	<u>N</u>				
<u>2020_HS</u>	<u>Huila_TRP</u>	<u>3</u>	<u>-76</u>	<u>10</u>	<u>1</u>
<u>2020_HS</u>	<u>Kerguelen_ANT</u>	<u>-49.25</u>	<u>69</u>	<u>10</u>	<u>3</u>
<u>2020_HS</u>	<u>Mocho_SAN</u>	<u>-40</u>	<u>-72</u>	<u>10</u>	<u>1</u>
<u>2020_HS</u>	<u>Olivine_NZL</u>	<u>-44.5</u>	<u>168.4</u>	<u>10</u>	<u>5</u>
<u>2020_HS</u>	<u>PascuaLama_SAN</u>	<u>-29.3</u>	<u>-70</u>	<u>10</u>	<u>1</u>
<u>2020_HS</u>	<u>Schiaparelli_SAN</u>	<u>-54.5</u>	<u>-70.8</u>	<u>10</u>	<u>1</u>
<u>2020_HN</u>	<u>Abramov_ASC</u>	<u>39.6</u>	<u>71.5</u>	<u>10</u>	<u>3</u>
<u>2020_HN</u>	<u>AkShirak_ASC</u>	<u>41.8</u>	<u>78.3</u>	<u>10</u>	<u>6</u>
<u>2020_HN</u>	<u>Altar_TRP</u>	<u>-1.7</u>	<u>-78.4</u>	<u>10</u>	<u>1</u>
<u>2020_HN</u>	<u>ChhotaShigri_ASW</u>	<u>32.2</u>	<u>77.5</u>	<u>10</u>	<u>2</u>
<u>2020_HN</u>	<u>Chimborazo_TRP</u>	<u>-1.5</u>	<u>-78.8</u>	<u>10</u>	<u>1</u>
<u>2020_HN</u>	<u>Disappointment_ALA</u>	<u>60.5</u>	<u>-138.5</u>	<u>10</u>	<u>2</u>
<u>2020_HN</u>	<u>Gangotri_ASE</u>	<u>33.8</u>	<u>76.3</u>	<u>10</u>	<u>2</u>
<u>2020_HN</u>	<u>Guliya_ASC</u>	<u>35.3</u>	<u>81.5</u>	<u>10</u>	<u>1</u>
<u>2020_HN</u>	<u>Hardangerjokulen_SCA</u>	<u>60.5</u>	<u>7.4</u>	<u>10</u>	<u>1</u>
<u>2020_HN</u>	<u>Kluane_ALA</u>	<u>60.9</u>	<u>-139.5</u>	<u>10</u>	<u>3</u>
<u>2020_HN</u>	<u>Koshik_ASW</u>	<u>36.9</u>	<u>75.4</u>	<u>10</u>	<u>1</u>
<u>2020_HN</u>	<u>Ladakh_ASW</u>	<u>34</u>	<u>77.5</u>	<u>10</u>	<u>1</u>
<u>2020_HN</u>	<u>Meager_WNA</u>	<u>50.6</u>	<u>-123.5</u>	<u>10</u>	<u>1</u>
<u>2020_HN</u>	<u>Zanskar_ASW</u>	<u>33.8</u>	<u>76.3</u>	<u>10</u>	<u>1</u>
<u>2021_HS</u>	<u>Astrolabe_ANT</u>	<u>-66.8</u>	<u>140</u>	<u>13</u>	<u>3</u>
<u>2021_HS</u>	<u>BallenyIsland1_ANT</u>	<u>-66.4</u>	<u>162.5</u>	<u>13</u>	<u>1</u>
<u>2021_HS</u>	<u>BallenyIsland2_ANT</u>	<u>-66.7</u>	<u>163.25</u>	<u>13</u>	<u>1</u>
<u>2021_HS</u>	<u>BallenyIsland3_ANT</u>	<u>-67.5</u>	<u>164.75</u>	<u>13</u>	<u>1</u>
<u>2021_HS</u>	<u>DrygalskiIsland_ANT</u>	<u>-65.7</u>	<u>92.5</u>	<u>13</u>	<u>2</u>
<u>2021_HS</u>	<u>LavoisierIsland_ANT</u>	<u>-66.2</u>	<u>-66.75</u>	<u>13</u>	<u>1</u>
<u>2021_HS</u>	<u>Marinelli_SAN</u>	<u>-55.5</u>	<u>-69.6</u>	<u>10</u>	<u>2</u>
<u>2021_HS</u>	<u>Montaguls_ANT</u>	<u>-58.5</u>	<u>-26.4</u>	<u>10</u>	<u>1</u>
<u>2021_HS</u>	<u>Roncagli_SAN</u>	<u>-54.75</u>	<u>-69.2</u>	<u>10</u>	<u>4</u>
<u>2021_HS</u>	<u>SouthOrkney_ANT</u>	<u>-60.7</u>	<u>-44.6</u>	<u>13</u>	<u>1</u>
<u>2021_HS</u>	<u>Viedma_SAN</u>	<u>-49.5</u>	<u>-73.1</u>	<u>10</u>	<u>2</u>
<u>2021_HS</u>	<u>WarsawIcefield_ANT</u>	<u>-62.2</u>	<u>-58.6</u>	<u>13</u>	<u>1</u>

References

- 566 Andreassen, L. M., Elvehøy, H., Kjøllmoen, B., and Engeset, R. V.: Reanalysis of long-term series of
glaciological and geodetic mass balance for 10 Norwegian glaciers, *The Cryosphere*, 10, 535–
568 552, <https://doi.org/10.5194/tc-10-535-2016>, 2016.
- 570 Andreassen, L. M., Nagy, T., Kjøllmoen, B., and Leigh, J. R.: An inventory of Norway’s glaciers and
ice-marginal lakes from 2018–19 Sentinel-2 data, *J. Glaciol.*, 1–22,
<https://doi.org/10.1017/jog.2022.20>, 2022.
- 572 Andreassen, L. M., Robson, B. A., Sjurset, K. H., Elvehøy, H., Kjøllmoen, B., and Carrivick, J. L.:
Spatio-temporal variability in geometry and geodetic mass balance of Jostedalbreen ice cap,
574 Norway, *Ann. Glaciol.*, 1–18, <https://doi.org/10.1017/aog.2023.70>, 2023.
- 576 Belart, J. M. C., Berthier, E., Magnússon, E., Anderson, L. S., Pálsson, F., Thorsteinsson, T., Howat, I.
M., Aðalgeirsdóttir, G., Jóhannesson, T., and Jarosch, A. H.: Winter mass balance of
578 Drangajökull ice cap (NW Iceland) derived from satellite sub-meter stereo images, *The
Cryosphere*, 11, 1501–1517, <https://doi.org/10.5194/tc-11-1501-2017>, 2017.
- 580 Beraud, L., Cusicanqui, D., Rabatel, A., Brun, F., Vincent, C., and Six, D.: Glacier-wide seasonal and
annual geodetic mass balances from Pléiades stereo images: application to the Glacier
d’Argentière, French Alps, *J. Glaciol.*, 69, 525–537, <https://doi.org/10.1017/jog.2022.79>, 2023.
- 582 Berthier, E., Vincent, C., Magnússon, E., Gunnlaugsson, Á. Þ., Pitte, P., Le Meur, E., Masiokas, M.,
Ruiz, L., Pálsson, F., Belart, J. M. C., and Wagnon, P.: Glacier topography and elevation
584 changes derived from Pléiades sub-meter stereo images, *The Cryosphere*, 8, 2275–2291,
<https://doi.org/10.5194/tc-8-2275-2014>, 2014.
- 586 Berthier, E., Floriciou, D., Gardner, A. S., Gourmelen, N., Jakob, L., Paul, F., Treichler, D., Wouters,
B., Belart, J. M. C., Dehecq, A., Dussaillant, I., Hugonnet, R., Käab, A., Krieger, L., Pálsson, F.,
588 and Zemp, M.: Measuring glacier mass changes from space—a review, *Rep. Prog. Phys.*, 86,
036801, <https://doi.org/10.1088/1361-6633/acf8e>, 2023.
- 590 Berthier, E., Vincent, C., and Six, D.: Exceptional thinning through the entire altitudinal range of
Mont-Blanc glaciers during the 2021/22 mass balance year, *J. Glaciol.*,
592 <https://doi.org/10.1017/jog.2023.100>, in press.
- 594 Bhattacharya, A., Bolch, T., Mukherjee, K., King, O., Menounos, B., Kapitsa, V., Neckel, N., Yang,
W., and Yao, T.: High Mountain Asian glacier response to climate revealed by multi-temporal
satellite observations since the 1960s, *Nat. Commun.*, 12, 4133,
596 <https://doi.org/10.1038/s41467-021-24180-y>, 2021.
- 598 [Bhushan, S., Shean, D., Alexandrov, O., and Henderson, S.: Automated digital elevation model
\(DEM\) generation from very-high-resolution Planet SkySat triplet stereo and video imagery,
ISPRS Journal of Photogrammetry and Remote Sensing, 173, 151–165,
<https://doi.org/10.1016/j.isprsjprs.2020.12.012>, 2021.](https://doi.org/10.1016/j.isprsjprs.2020.12.012)
- 600 Błaszczuk, M., Ignatiuk, D., Grabiec, M., Kolondra, L., Laska, M., Decaux, L., Jania, J., Berthier, E.,
602 Luks, B., Barzycka, B., and Czapla, M.: Quality Assessment and Glaciological Applications of
Digital Elevation Models Derived from Space-Borne and Aerial Images over Two Tidewater
604 Glaciers of Southern Spitsbergen, *Remote Sens.*, 11, 1121,
<https://doi.org/10.3390/rs11091121>, 2019.
- 606 Brun, F., Buri, P., Miles, E. S., Wagnon, P., Steiner, J., Berthier, E., Ragettli, S., Kraaijenbrink, P.,
Immerzeel, W. W., and Pellicciotti, F.: Quantifying volume loss from ice cliffs on debris-
608 covered glaciers using high resolution terrestrial and aerial photogrammetry, *J. Glaciol.*, 62,
684–695, <https://doi.org/10.1017/jog.2016.54>, 2016.
- 610 Brun, F., Berthier, E., Wagnon, P., Käab, A., and Treichler, D.: A spatially resolved estimate of High
Mountain Asia glacier mass balances from 2000 to 2016, *Nat. Geosci.*, 10, 668–673,
612 <https://doi.org/10.1038/ngeo2999>, 2017.
- 614 Deschamps-Berger, C., Gascoin, S., Berthier, E., Deems, J., Gutmann, E., Dehecq, A., Shean, D., and
Dumont, M.: Snow depth mapping from stereo satellite imagery in mountainous terrain:

616 evaluation using airborne laser-scanning data, *The Cryosphere*, 14, 2925–2940,
<https://doi.org/10.5194/tc-14-2925-2020>, 2020.

618 Dussailant, I., Berthier, E., and Brun, F.: Geodetic Mass Balance of the Northern Patagonian
Icefield from 2000 to 2012 Using Two Independent Methods, *Front. Earth Sci.*, 6, 8,
<https://doi.org/10.3389/feart.2018.00008>, 2018.

620 [ESA and Airbus: Copernicus DEM – Global and European Digital Elevation Model \(COP-DEM\), ESA,
| Copernicus \[data set\], <https://doi.org/10.5270/ESA-c5d3d65>, 2022.](#)

622 Falaschi, D., Berthier, E., Belart, J. M. C., Bravo, C., Castro, M., Durand, M., and Villalba, R.:
Increased mass loss of glaciers in Volcán Domuyo (Argentinian Andes) between 1962 and
624 2020, revealed by aerial photos and satellite stereo imagery, *J. Glaciol.*, 69, 40–56,
<https://doi.org/10.1017/jog.2022.43>, 2023.

626 Franks, S. and Rengarajan, R.: Evaluation of Copernicus DEM and Comparison to the DEM Used for
Landsat Collection-2 Processing, *Remote Sens.*, 15, <https://doi.org/10.3390/rs15102509>,
628 2023.

Gardelle, J., Berthier, E., Arnaud, Y., and Kääb, A.: Region-wide glacier mass balances over the
630 Pamir-Karakoram-Himalaya during 1999–2011, *The Cryosphere*, 7, 1263–1286,
<https://doi.org/10.5194/tc-7-1263-2013>, 2013.

632 Gleyzes, M. A., Perret, L., and Kubik, P.: Pléiades system architecture and main performances, *Int
Arch Photogramm. Remote Sens. Informat. Sci.*, 39, 537–542, 2012.

634 GTN-G: GTN-G Glacier Regions. Global Terrestrial Network for Glaciers.,
<https://doi.org/10.5904/gtng-glacreg-2023-07>, 2023.

636 Hirschmuller, H.: Stereo Processing by Semiglobal Matching and Mutual Information, *IEEE Trans
Pattern Anal. Mach. Intell.*, 30, 328–341, 2008.

638 [Holzer, N., Vijay, S., Yao, T., Xu, B., Buchroithner, M., and Bolch, T.: Four decades of glacier
| variations at Muztagh Ata \(eastern Pamir\): a multi-sensor study including Hexagon KH-9 and
640 Pléiades data, *The Cryosphere*, 9, 2071–2088, <https://doi.org/10.5194/tc-9-2071-2015>, 2015.](#)

642 Howat, I. M., Porter, C., Smith, B. E., Noh, M.-J., and Morin, P.: The Reference Elevation Model of
Antarctica, *The Cryosphere*, 13, 665–674, <https://doi.org/10.5194/tc-13-665-2019>, 2019.

644 Hugonnet, R., McNabb, R., Berthier, E., Menounos, B., Nuth, C., Girod, L., Farinotti, D., Huss, M.,
Dussailant, I., Brun, F., and Kääb, A.: Accelerated global glacier mass loss in the early twenty-
first century, *Nature*, 592, 726–731, <https://doi.org/10.1038/s41586-021-03436-z>, 2021.

646 Hugonnet, R., Brun, F., Berthier, E., Dehecq, A., Mannerfelt, E. S., Eckert, N., and Farinotti, D.:
Uncertainty analysis of digital elevation models by spatial inference from stable terrain, *IEEE
648 J. Sel. Top. Appl. Earth Obs. Remote Sens.*, 15, 6456–6472,
<https://doi.org/10.1109/JSTARS.2022.3188922>, 2022.

650 Kääb, A., Jacquemart, M., Gilbert, A., Leinss, S., Girod, L., Huggel, C., Falaschi, D., Ugalde, F.,
Petrakov, D., Chernomorets, S., Dokukin, M., Paul, F., Gascoin, S., Berthier, E., and Kargel, J.
652 S.: Sudden large-volume detachments of low-angle mountain glaciers – more frequent than
thought?, *The Cryosphere*, 15, 1751–1785, <https://doi.org/10.5194/tc-15-1751-2021>, 2021.

654 Lacroix, P.: Landslides triggered by the Gorkha earthquake in the Langtang valley, volumes and
initiation processes, *Earth Planets Space*, 68, 1–10, [https://doi.org/10.1186/s40623-016-
0423-3](https://doi.org/10.1186/s40623-016-

656 0423-3), 2016.

658 Lebègue, L., Greslou, D., Blanchet, G., Lussy, F., Fourest, S., Martin, V., Latry, C., Kubik, P., Delvit, J.-
M., Dechoz, C., and Amberg, V.: Pléiades-HR satellites image quality commissioning, *Rev. Fr.
Photogramm. Télédétection*, 5–10, <https://doi.org/10.52638/rfpt.2015.137>, 2015.

660 Loriaux, T. and Ruiz, L.: Spatio-Temporal Distribution of Supra-Glacial Ponds and Ice Cliffs on Verde
Glacier, Chile, *Front. Earth Sci.*, 9, 448, <https://doi.org/10.3389/feart.2021.681071>, 2021.

662 Małeck, J.: Recent contrasting behaviour of mountain glaciers across the European High Arctic
revealed by ArcticDEM data, *The Cryosphere*, 16, 2067–2082, [https://doi.org/10.5194/tc-16-
2067-2022](https://doi.org/10.5194/tc-16-

664 2067-2022), 2022.

666 Marti, R., Gascoin, S., Berthier, E., de Pinel, M., Houet, T., and Laffly, D.: Mapping snow depth in
open alpine terrain from stereo satellite imagery, *The Cryosphere*, 10, 1361–1380,

<https://doi.org/10.5194/tc-10-1361-2016>, 2016.

668 Miles, E. S., Watson, C. S., Brun, F., Berthier, E., Esteves, M., Quincey, D. J., Miles, K. E., Hubbard,

670 B., and Wagnon, P.: Glacial and geomorphic effects of a supraglacial lake drainage and

outburst event, Everest region, Nepal Himalaya, *The Cryosphere*, 12, 3891–3905,

<https://doi.org/10.5194/tc-12-3891-2018>, 2018.

672 Millan, R., Mouginot, J., Rabatel, A., and Morlighem, M.: Ice velocity and thickness of the world’s

glaciers, *Nat. Geosci.*, 15, 124–129, <https://doi.org/10.1038/s41561-021-00885-z>, 2022.

674 Nuth, C. and Kääb, A.: Co-registration and bias corrections of satellite elevation data sets for

quantifying glacier thickness change, *The Cryosphere*, 5, 271–290,

676 <https://doi.org/10.5194/tcd-4-2013-2010>, 2011.

Paul, F., Frey, H., and Le Bris, R.: A new glacier inventory for the European Alps from Landsat TM

678 scenes of 2003: Challenges and results, *Ann. Glaciol.*, 52, 144–152, 2011.

Pelto, M. S.: Forecasting temperate alpine glacier survival from accumulation zone observations,

680 *Cryosphere*, 4, 67–75, 2010.

| [Pelto, B. M., Menounos, B., and Marshall, S. J.: Multi-year evaluation of airborne geodetic surveys](https://doi.org/10.5194/tc-13-1709-2019)

682 [to estimate seasonal mass balance, Columbia and Rocky Mountains, Canada, *The Cryosphere*, 13, 1709–1727, https://doi.org/10.5194/tc-13-1709-2019, 2019.](https://doi.org/10.5194/tc-13-1709-2019)

|

684 Pfeffer, W. T., Arendt, A. A., Bliss, A., Bolch, T., Cogley, J. G., Gardner, A. S., Hagen, J.-O., Hock, R.,

Kaser, G., Kienholz, C., Miles, E. S., Moholdt, G., Moelg, N., Paul, F., Radic, V., Rastner, P.,

686 Raup, B. H., Rich, J., Sharp, M. J., Andeassen, L. M., Bajracharya, S., Barrand, N. E., Beedle, M.

J., Berthier, E., Bhambri, R., Brown, I., Burgess, D. O., Burgess, E. W., Cawkwell, F., Chinn, T.,

688 Copland, L., Cullen, N. J., Davies, B., De Angelis, H., Fountain, A. G., Frey, H., Giffen, B. A.,

Glasser, N. F., Gurney, S. D., Hagg, W., Hall, D. K., Haritashya, U. K., Hartmann, G., Herreid, S.,

690 Howat, I., Jiskoot, H., Khromova, T. E., Klein, A., Kohler, J., König, M., Krieger, D., Kutuzov, S.,

Lavrentiev, I., Le Bris, R., Li, X., Manley, W. F., Mayer, C., Menounos, B., Mercer, A., Mool, P.,

692 Negrete, A., Nosenko, G., Nuth, C., Osmonov, A., Pettersson, R., Racoviteanu, A., Ranzi, R.,

Sarikaya, M. A., Schneider, C., Sigurdsson, O., Sirguey, P., Stokes, C. R., Wheate, R., Wolken, G.

694 J., Wu, L. Z., and Wyatt, F. R.: The Randolph Glacier Inventory: a globally complete inventory

of glaciers, *J. Glaciol.*, 60, 537–552, <https://doi.org/10.3189/2014JoG13J176>, 2014.

696 Piermattei, L., Marty, M., Ginzler, C., Pöchltrager, M., Karel, W., Ressler, C., Pfeifer, N., and Hollaus,

M.: Pléiades satellite images for deriving forest metrics in the Alpine region, *Int. J. Appl. Earth*

698 *Obs. Geoinformation*, 80, 240–256, <https://doi.org/10.1016/j.jag.2019.04.008>, 2019.

Pope, A., Rees, W. G., Fox, A. J., and Fleming, A.: Open Access Data in Polar and Cryospheric

700 Remote Sensing, *Remote Sens.*, 6, 6183–6220, <https://doi.org/10.3390/rs6076183>, 2014.

Porter, C., Morin, P., Howat, I., Noh, M.-J., Bates, B., Peterman, K., Keeseey, S., Schlenk, M.,

702 Gardiner, J., Tomko, K., Willis, M., Kelleher, C., Cloutier, M., Husby, E., Foga, S., Nakamura, H.,

Platson, M., Wethington, M., Jr., Williamson, C., Bauer, G., Enos, J., Arnold, G., Kramer, W.,

704 Becker, P., Doshi, A., D’Souza, C., Cummins, P., Laurier, F., and Bojesen, M.: ArcticDEM, ,

<https://doi.org/10.7910/DVN/OHHUKH>, 2018.

706 Rabatel, A., Letréguilly, A., Dedieu, J.-P., and Eckert, N.: Changes in glacier equilibrium-line altitude

in the western Alps from 1984 to 2010: evaluation by remote sensing and modeling of the

708 morpho-topographic and climate controls, *The Cryosphere*, 7, 1455–1471,

<https://doi.org/10.5194/tc-7-1455-2013>, 2013.

710 RGI 7.0 Consortium: Randolph Glacier Inventory - A Dataset of Global Glacier Outlines, Version

7.0., 2023.

712 Rounce, D. R., Hock, R., Maussion, F., Hugonnet, R., Kochtitzky, W., Huss, M., Berthier, E.,

Brinkerhoff, D., Compagno, L., Copland, L., Farinotti, D., Menounos, B., and McNabb, R. W.:

714 Global glacier change in the 21st century: Every increase in temperature matters, *Science*,

379, 78–83, <https://doi.org/10.1126/science.abo1324>, 2023.

716 Sato, Y., Fujita, K., Inoue, H., Sunako, S., Sakai, A., Tsushima, A., Podolskiy, E. A., Kayastha, R., and

Kayastha, R. B.: Ice Cliff Dynamics of Debris-Covered Trakarding Glacier in the Rolwaling

718 Region, Nepal Himalaya, *Front. Earth Sci.*, 9, <https://doi.org/10.3389/feart.2021.623623>,

2021.

- 720 Shean, D. E., Alexandrov, O., Moratto, Z. M., Smith, B. E., Joughin, I. R., Porter, C., and Morin, P.:
722 An automated, open-source pipeline for mass production of digital elevation models (DEMs)
724 from very-high-resolution commercial stereo satellite imagery, *ISPRS J. Photogramm. Remote*
726 *Sens.*, 116, 101–117, <https://doi.org/10.1016/j.isprsjprs.2016.03.012>, 2016.
- 724 Shean, D. E., Bhushan, S., Montesano, P., Rounce, D. R., Arendt, A., and Osmanoglu, B.: A
726 Systematic, Regional Assessment of High Mountain Asia Glacier Mass Balance, *Front. Earth*
728 *Sci.*, 7, 363, <https://doi.org/10.3389/feart.2019.00363>, 2020.
- 728 [Shean, D., Bhushan, S., Lilien, D., Knuth, F., Schwat, E., Meyer, J., Sharp, M., and Hu, M.:
dshean/demcoreg: v1.1.1 Compatibility and doc improvements, ,
<https://doi.org/10.5281/zenodo.7730376>, 2023.](https://doi.org/10.5281/zenodo.7730376)
- 730 Shugar, D. H., Jacquemart, M., Shean, D., Bhushan, S., Upadhyay, K., Sattar, A., Schwanghart, W.,
732 McBride, S., de Vries, M. V. W., Mergili, M., Emmer, A., Deschamps-Berger, C., McDonnell, M.,
734 Bhambri, R., Allen, S., Berthier, E., Carrivick, J. L., Clague, J. J., Dokukin, M., Dunning, S. A.,
736 Frey, H., Gascoin, S., Haritashya, U. K., Huggel, C., Käab, A., Kargel, J. S., Kavanaugh, J. L.,
738 Lacroix, P., Petley, D., Rupper, S., Azam, M. F., Cook, S. J., Dimri, A. P., Eriksson, M., Farinotti,
D., Fiddes, J., Gnyawali, K. R., Harrison, S., Jha, M., Koppes, M., Kumar, A., Leinss, S., Majeed,
U., Mal, S., Muhuri, A., Noetzli, J., Paul, F., Rashid, I., Sain, K., Steiner, J., Ugalde, F., Watson, C.
S., and Westoby, M. J.: A massive rock and ice avalanche caused the 2021 disaster at Chamoli,
Indian Himalaya, *Science*, 373, 300, <https://doi.org/10.1126/science.abh4455>, 2021.
- 740 Toutin, T.: Three-dimensional topographic mapping with ASTER stereo data in rugged topography,
742 *IEEE Trans. Geosci. Remote Sens.*, 40, 2241–2247,
<https://doi.org/10.1109/TGRS.2002.802878>, 2002.
- 742 Wagnon, P., Brun, F., Khadka, A., Berthier, E., Shrestha, D., Vincent, C., Arnaud, Y., Six, D., Dehecq,
744 A., Ménégoz, M., and Jomelli, V.: Reanalysing the 2007–19 glaciological mass-balance series
of Mera Glacier, Nepal, Central Himalaya, using geodetic mass balance, *J. Glaciol.*, 67, 117–
125, <https://doi.org/10.1017/jog.2020.88>, 2021.
- 746 Willis, M. J., Herried, B. G., Bevis, M. G., and Bell, R. E.: Recharge of a subglacial lake by surface
meltwater in northeast Greenland, *Nature*, 518, 223–227, 2015.
- 748 Zemp, M., Thibert, E., Huss, M., Stumm, D., Rolstad Denby, C., Nuth, C., Nussbaumer, S. U.,
750 Moholdt, G., Mercer, A., Mayer, C., Joerg, P. C., Jansson, P., Hynek, B., Fischer, A., Escher-
752 Vetter, H., Elvehøy, H., and Andreassen, L. M.: Reanalysing glacier mass balance
measurement series, *The Cryosphere*, 7, 1227–1245, [https://doi.org/10.5194/tc-7-1227-](https://doi.org/10.5194/tc-7-1227-2013)
2013, 2013.